CrossMark

J. Fluid Mech. (2018), *vol.* 845, *pp.* 682–712. © Cambridge University Press 2018
doi:10.1017/jfm.2018.265

Wave radiation and diffraction by a circular cylinder submerged below an ice sheet with a crack

Zhi Fu Li[1], Guo Xiong Wu[1,2,†] and Chun Yan Ji[1]

[1]School of Naval Architecture and Ocean Engineering, Jiangsu University of Science and Technology, Zhenjiang 212003, China

[2]Department of Mechanical Engineering, University College London, Torrington Place, London WC1E 7JE, UK

(Received 10 October 2017; revised 26 February 2018; accepted 21 March 2018; first published online 30 April 2018)

Wave radiation and diffraction by a circular cylinder submerged below an ice sheet with a crack are considered based on the linearized velocity potential theory together with multipole expansion. The solution starts from the potential due to a single source, or the Green function satisfying both the ice sheet condition and the crack condition, as well as all other conditions apart from that on the body surface. This is obtained in an integral form through Fourier transform, in contrast to what has been obtained previously in which the Green function is in the series form based on the method of matched eigenfunction expansion in each domain on both sides of the crack. The multipole expansion is then constructed through direct differentiation of the Green function with respect to the source position, rather than treating each multipole as a separate problem. The use of the Green function enables the problem of wave diffraction by the crack in the absence of the body to be solved directly. For the circular cylinder, wave radiation and diffraction problems are solved by applying the body surface boundary condition to the multipole expansion, through which the unknown coefficients are obtained. Extensive results are provided for the added mass and damping coefficient as well as the exciting force. When the cylinder is away from the crack, a wide spacing approximation method is used, which is found to provide accurate results apart from when the cylinder is quite close to the crack.

Key words: ice sheets, wave scattering, wave-structure interactions

1. Introduction

As the Arctic region may become a possible shipping route (Smith & Stephenson 2013), there has been an increasing interest in understanding the behaviour of a ship or other structure in water covered by an ice sheet over a large extent. The motion of a ship in such an environment is expected to be very different from that of a ship in the open sea.One of the main reasons is that the geophysical condition in the

† Email address for correspondence: g.wu@ucl.ac.uk

https://doi.org/10.1017/jfm.2018.265 Published online by Cambridge University Press

Arctic is different, or the typical wave which the ship encounters is different. Another reason is that when the ship is set into motion by an incoming wave, its radiated wave will be reflected by the ice sheet. It will propagate back to the ship and have further interactions with the ship. This makes interactions of a ship with the external environment more complex.

The work on wave/ice interactions without a floating body in the context of geophysics started very early. Following the work of Greenhill (1887), when the horizontal dimension of the ice sheet is much larger than its vertical dimension, it is very common to use the elastic plate model for the sea ice. In many cases, the fluid flow due to wave/ice interaction can be modelled by the linear velocity potential theory. These assumptions are valid for a wide range of problems in the polar region, as explained in the review papers by Squire *et al.* (1995) and Squire (2007, 2011). Based on this model, Fox & Squire (1990) considered the problem of wave propagating from open sea to the shore fast ice. They obtained the reflection and transmission coefficients for a wave into a semi-infinite ice sheet. The wave direction was normal to the edge of ice sheet, and the problem was two-dimensional and was solved through matched eigenfunction expansions (MEE), in which the unknowns were found by numerically minimizing the errors in the matching conditions and edge conditions. This was then extended to the oblique incident wave by Fox & Squire (1994). A similar problem was considered by Sahoo, Yip & Chwang (2001), where the unknowns in the eigenfunction expansions were found through introducing an inner product of orthogonality. The problem was also solved through the Wiener–Hopf method initiated by Evans & Davies (1968), as done by Balmforth & Craster (1999), Chung & Fox (2002) and Tkacheva (2004). For an ice sheet of finite length or an ice floe, Meylan & Squire (1993) obtained an approximate solution based on the large length assumption. They provided an explicit equation which showed that there would be an infinite number of discrete frequencies at which the reflection coefficient would be zero or perfect transmission would occur. The problem was also solved without the large length assumption by Meylan & Squire (1994) through the Green function method. Chung & Linton (2005) considered an open lead or polynya, while Williams & Squire (2006) considered the case in which the surface of polynya was refrozen. Zero reflection was also found in these cases. For an infinite ice sheet with a crack, Barrett & Squire (1996) solved the wave reflection problem of finite depth through an MEE method similar to that in Fox & Squire (1994). For infinite water depth, by using the Green function for the ice sheet without crack, Squire & Dixon (2000) solved the problem for the normal incident wave, while Williams & Squire (2002) did the same for the oblique incident wave. By separating the problem into the symmetric and antisymmetric parts, Evans & Porter (2003) obtained the solution for an oblique wave in a series form for finite water depth, and localized edge waves travelling along the crack were found to be possible. The problem was further extended to the multiple parallel cracks of infinite length by Porter & Evans (2006), and to cracks of finite length by Porter & Evans (2007).

The work with the body present in the wave/ice interaction problem started relatively later. Das & Mandal (2006) used the multipole expansion method for wave scattering by a circular cylinder submerged below a surface entirely covered by an ice sheet. Wave reflection and transmission coefficients were obtained for various ice flexural stiffnesses. Sturova (2014*b*) obtained the Green function for the water surface covered by a semi-infinite ice sheet through the MEE method. The unknown coefficients were found through a matrix equation which was resolved for different source positions. The wave radiation problem by a submerged cylinder was solved

https://doi.org/10.1017/jfm.2018.265 Published online by Cambridge University Press

through the boundary element method. This was further extended to the problem for infinitely extended ice sheet with a crack (Sturova 2015*a*), and an ice floe or a polynya (Sturova 2015*b*). The effect of an ice floe on the hydrodynamic coefficients of a submerged body was also considered by Tkacheva (2015), in which the Green function was obtained through the Wiener–Hopf technique. For a body floating on a polynya, Ren, Wu & Thomas (2016) solved the problem for a rectangular body using the MEE method, while Li, Shi & Wu (2018) used a hybrid eigenfunction expansion and boundary element method and solved the problem for a floating body of arbitrary shape. Using the wide polynya approximation, Li, Shi & Wu (2017*a*) solved the problem of a body floating on polynya based on the solutions for polynya without a body and a floating body without ice. Explicit equations were derived, which uncovered the mechanism for the oscillatory behaviours of the hydrodynamic force and the body motion. The nonlinear effect of the body position during its motion was considered by Li, Shi & Wu (2017*b*) through using the multipole expansion for a circular cylinder.

In this paper, we consider the problem of wave interaction with a circular cylinder submerged in water covered by an ice sheet with a crack. Although the problem is two-dimensional (2-D), as in common in other physical problem, such a simplification is appropriate when the variation of the physical parameters in the third dimension is much smaller than that in the other two. Also the obtained results often shed some important insights into general three-dimensional problems. For this reason, the 2-D problem has been considered widely in the context of wave/ice interaction (Squire 2007). For the problems in naval architecture, the 2-D solution for each cross-section of a ship can be incorporated into the strip method (Newman 1977) and the so-called 2-D+t method (Faltinsen 2005) used as a practical design tool.

There are some significantly different features between the present work and those done previously. Firstly, we shall derive the Green function, or the potential due to a single source, which satisfies both the ice sheet and crack condition. This allows us to obtain the solution for wave diffraction by the ice crack directly, while this problem was solved by Evans & Porter (2003) using the Green function for the ice sheet without a crack. We shall show that our result is identical to theirs for this particular case. Secondly, we should mention that the Green function which satisfies both the ice sheet and crack condition was obtained by Sturova (2015*a*). She started the solution from the Green function without the crack. To satisfy the condition at the crack, expansions of the potential based on MEE were used on both sides of the crack. The series was then truncated at a finite number. The coefficients in the expansions were found through the solution of the matrix equation obtained from matching conditions at the interface. This is different from the free surface problem where the coefficients are given explicitly. The procedure was repeated for each different location of the source whose horizontal coordinate should not be the same as that of the crack. Here we shall use Fourier transform and the Green function is obtained in a simple integral form, which does not require re-derivation when the source is at a different point. Also infinite water depth is merely a special case of the present formation, for which the MEE is no longer applicable. It should be emphasized that the integral form of the Green function may be standard for a homogenous upper surface condition, as in Evans & Porter (2003) for an infinite ice sheet without a crack. However its derivation for the ice sheet with a crack is less straightforward and therefore it is one of the principal contributions of the present paper. Thirdly, in addition to being used more efficiently than the series form of Sturova (2015*a*) in the boundary element method for a body of arbitrary shape, from

https://doi.org/10.1017/jfm.2018.265 Published online by Cambridge University Press

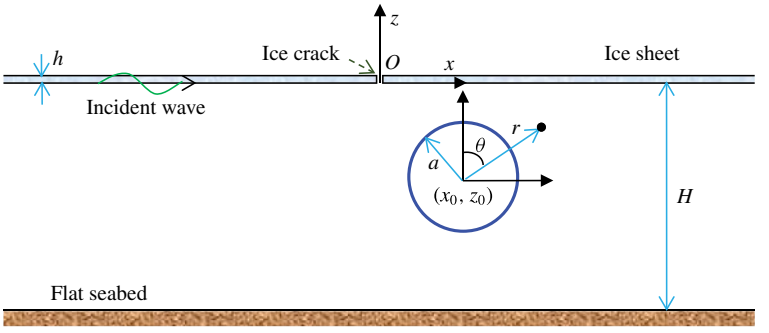


FIGURE 1. (Colour online) Coordinate system and sketch of the problem.

the derived Green function, we may obtain the potential due to multipoles through direct differentiation with respect to the position of the source. The method was initiated by Ursell (1949, 1950) to solve the water wave interaction problem with a floating semi-circular cylinder and a submerged circular cylinder. His pioneering work had a major impact in naval architecture, especially in the development of strip theory for ship motion in waves. However, the equivalent multipole expansion method has not been developed in the problem of an ice sheet with a crack. Some attempts were made to use the multipole expansion method for a circular cylinder near the edge of a semi-infinite sheet (Sturova 2014*a*). However, the coefficients in the series expansion for each multipole were obtained separately. Here by taking the advantage of the simple form of the newly derived Green function, the multipole is constructed directly through differentiation of the Green function with respect to the source position. Finally, a wide spacing approximation method (Srokosz & Evans 1979) is adopted for this type of problem. This enables us to obtain accurate results from the solution for a cylinder without the crack and the solution for a crack without the cylinder, similar to that for a body in a wide polynya (Li *et al.* 2017*a*). It also enables us to have some deep understanding of physical nature of the problem.

The paper is organized as follows. A description of the linearized velocity potential problem for the ice sheet with a crack is presented in § 2. The Green function, or the potential due to an oscillating source, is derived in § 3.1, from which the multipole expansion is constructed in § 3.2. The potentials for the radiation and diffraction problems of a submerged circular cylinder are then constructed in §§ 3.3 and 3.4 respectively. Special cases including the wide spacing approximation and deep water limit are considered in § 3.5. Results are presented and discussed in § 4, followed by the conclusion in § 5. In appendices A and B, the far field formulas for damping coefficient and wave exciting force are presented respectively, while in appendix C the Haskind relation for the wave exciting force is derived.

2. Mathematical model

We consider the problem of wave interaction with a circular cylinder of radius a submerged in water covered by an ice sheet with a crack, as sketched in figure 1. A Cartesian coordinate system O–xz is defined, with the x-axis along the undisturbed mean upper surface, and the z-axis pointing vertically upwards. The ice sheet with uniform properties is extended from $x = -\infty$ to $x = +\infty$. Its draught is assumed to be zero, and the crack is assumed to be located at $x = 0$, as shown in the figure.

https://doi.org/10.1017/jfm.2018.265 Published online by Cambridge University Press

The fluid with density ρ and depth H is assumed to be inviscid, incompressible and homogeneous, and its motion to be irrotational. Thus the velocity potential Φ can be introduced to describe the fluid flow. Under the assumption that the amplitude of the wave motion is small compared to its length and the dimension of the body, the linearized velocity potential theory can be further used. Based on the assumption that the motion is sinusoidal in time with frequency ω, the total velocity potential can be written in the following form

$$\Phi(x, z, t) = \mathrm{Re}\left[\alpha_0\phi_0(x, z)\mathrm{e}^{\mathrm{i}\omega t} + \sum_{j=1}^{2} \mathrm{i}\omega\alpha_j\phi_j(x, z)\mathrm{e}^{\mathrm{i}\omega t}\right], \tag{2.1}$$

where the scattering potential ϕ_0 contains the incident potential ϕ_I and diffracted potential ϕ_D, α_0 is the amplitude of the incident wave; ϕ_j $(j = 1, 2)$ is the radiation potential due to body oscillation with complex amplitude α_j in the x and z directions respectively. The rotational mode is not included in (2.1) as the rotation of a circular cylinder about its centre does not disturb the fluid. Mass conservation requires that the potential ϕ_j satisfies the Laplace's equation

$$\nabla^2\phi_j = 0, \quad (j = 0, 1, 2), \tag{2.2}$$

throughout the fluid. The ice sheet is modelled as a continuous elastic plate with uniform properties, i.e. thickness h, density ρ_0, Young's modulus E, Poisson's ratio ν are all constant. Thus the boundary condition on the ice sheet can be written as (Fox & Squire 1990)

$$\left(L\frac{\partial^4}{\partial x^4} - m\omega^2 + \rho g\right)\frac{\partial\phi_j}{\partial z} - \rho\omega^2\phi_j = 0, \quad (|x| > 0, z = 0), \tag{2.3}$$

where $L = Eh^3/[12(1 - \nu^2)]$ is the effective flexural rigidity of the ice sheet, and $m = h\rho_0$ is its mass per unit area. As the ice sheet has a crack at $x = 0$, zero bending moment and shear force are assumed there (Squire 2007). This leads to the following two conditions

$$\frac{\partial^2}{\partial x^2}\left(\frac{\partial\phi_j}{\partial z}\right) = 0 \quad \text{and} \quad \frac{\partial^3}{\partial x^3}\left(\frac{\partial\phi_j}{\partial z}\right) = 0, \quad (x = 0, z = 0). \tag{2.4a,b}$$

It may be noticed that we can also impose other conditions at the crack, e.g. the two semi-infinite sheets are hinged or connected by springs. These can be done through specifying proper combinations of the displacements, slopes, bending moments and shear forces, on both sides of the crack. The impermeable condition on the body surface is

$$\frac{\partial\phi_0}{\partial n} = 0 \quad \text{and} \quad \frac{\partial\phi_j}{\partial n} = n_j, \quad (j = 1, 2), \tag{2.5a,b}$$

where n_1 and n_2 are the x, z components of the unit normal vector $\boldsymbol{n}$ pointing into the body. On the flat seabed, the following condition should be also enforced

$$\frac{\partial\phi_j}{\partial z} = 0, \quad (z = -H). \tag{2.6}$$

https://doi.org/10.1017/jfm.2018.265 Published online by Cambridge University Press

The radiation condition at infinity requires the wave to propagate outwards

$$\lim_{x\to\pm\infty}\left(\frac{\partial\phi_D}{\partial x}\pm \mathrm{i}\lambda\phi_D\right)=0 \quad \text{and} \quad \lim_{x\to\pm\infty}\left(\frac{\partial\phi_j}{\partial x}\pm \mathrm{i}\lambda\phi_j\right)=0, \quad (j=1,2), \tag{2.7a,b}$$

where λ is the purely positive real root of the dispersion equation for a flexural gravity wave in the ice sheet, or

$$K(\omega,\lambda)\equiv(L\lambda^4+\rho g-m\omega^2)\lambda\tanh(\lambda H)-\rho\omega^2=0. \tag{2.8}$$

3. Solution procedures

3.1. *Velocity potential due to a single source: the Green function*

The Green function $G(x, z; x_0, z_0)$ is defined as the velocity potential at point $p(x, z)$ due to a source at $q(x_0, z_0)$. It then satisfies the following equation

$$\nabla^2 G=2\pi\delta(x-x_0)\delta(z-z_0), \tag{3.1}$$

and the same boundary conditions as those in (2.3), (2.4), (2.6) and (2.7). Here, $\delta(x)$ is the Dirac delta function. In order to derive G, we shall use the Fourier transform

$$\tilde{G}=\frac{1}{2\pi}\int_{-\infty}^{+\infty} G\mathrm{e}^{-\mathrm{i}kx}\,\mathrm{d}x. \tag{3.2}$$

We may replace ω in (2.1) with $\gamma=\omega-\mathrm{i}\epsilon$, where $\epsilon\to 0^+$ (Lighthill 1978). For a non-zero ϵ, $G\to 0$ when $|x|\to\infty$, and the radiation condition in (2.7) will be satisfied when ϵ is taken to be zero. Applying (3.2) to (3.1), we obtain

$$-k^2\tilde{G}+\frac{\partial^2\tilde{G}}{\partial z^2}=\delta(z-z_0)\mathrm{e}^{-\mathrm{i}kx_0}. \tag{3.3}$$

Here we introduce

$$z_>=\max(z,z_0) \quad \text{and} \quad z_<=\min(z,z_0). \tag{3.4a,b}$$

Then the solution for (3.3) with the boundary condition in (2.6) can be written in the following form

$$\tilde{G}=\frac{\mathrm{e}^{-\mathrm{i}kx_0}}{k}[\alpha k\cosh(kz_>)+\beta\sinh(kz_>)]Z(z_<), \tag{3.5}$$

where α and β are two unknown constants to be solved,

$$Z(z)=\cosh[k(z+H)]. \tag{3.6}$$

Integrating (3.3) with respect to z from z_0^- to z_0^+, we have

$$\left(\frac{\partial\tilde{G}}{\partial z}\right)_{z=z_0^-}^{z=z_0^+}=\mathrm{e}^{-\mathrm{i}kx_0}. \tag{3.7}$$

Substituting (3.5) into (3.7), we obtain

$$-\alpha k\sinh(kH)+\beta\cosh(kH)=1. \tag{3.8}$$

https://doi.org/10.1017/jfm.2018.265 Published online by Cambridge University Press

Fourier transform can also be applied to the boundary condition on the ice sheet in (2.3). We have

$$\tilde{U} + (\rho g - m\gamma^2)\frac{\partial \tilde{G}}{\partial z} - \rho\gamma^2 \tilde{G} = 0, \tag{3.9}$$

where

$$\tilde{U} = \frac{L}{2\pi}\int_{-\infty}^{+\infty} \frac{\partial^5 G}{\partial x^4 \partial z} \mathrm{e}^{-\mathrm{i}kx}\,\mathrm{d}x. \tag{3.10}$$

Through integrating by parts and using the condition of $G \to 0$ at $|x| \to \infty$ when ϵ is non-zero, (3.10) can be given as

$$\tilde{U} = \frac{L}{2\pi}\left[\left(\frac{\partial^4 G}{\partial x^3 \partial z} + \mathrm{i}k\frac{\partial^3 G}{\partial x^2 \partial z} - k^2\frac{\partial^2 G}{\partial x \partial z} - \mathrm{i}k^3\frac{\partial G}{\partial z}\right)\mathrm{e}^{-\mathrm{i}kx}\right]_{x=0^+}^{x=0^-} + Lk^4\frac{\partial \tilde{G}}{\partial z}. \tag{3.11}$$

At the ice crack, we have condition (2.4). It is expected that the displacements and the slopes on both sides of the crack are discontinuous. Thus we may write

$$\left(\frac{\partial G}{\partial z}\right)_{x=0^+}^{x=0^-} = A, \quad (z=0), \tag{3.12}$$

$$\left(\frac{\partial^2 G}{\partial x \partial z}\right)_{x=0^+}^{x=0^-} = B, \quad (z=0). \tag{3.13}$$

Then (3.11) can be written as

$$\tilde{U} = -\frac{L}{2\pi}(\mathrm{i}k^3 A + k^2 B) + Lk^4\frac{\partial \tilde{G}}{\partial z}. \tag{3.14}$$

It may be noticed that for crack conditions different from those in (3.12) and (3.13), a similar procedure may be followed, leading to a different form of (3.14). Substituting (3.5) together with (3.14) into (3.9) and invoking (3.8), we obtain

$$\alpha = \frac{L}{2\pi}\frac{\mathrm{i}k^3 A + k^2 B}{K(\gamma, k)Z(z_0)}\mathrm{e}^{\mathrm{i}kx_0} - \frac{Lk^4 + \rho g - m\gamma^2}{K(\gamma, k)Z(0)}, \tag{3.15}$$

$$\beta = \frac{L}{2\pi}\frac{(\mathrm{i}k^3 A + k^2 B)Z'(0)}{K(\gamma, k)Z(z_0)Z(0)}\mathrm{e}^{\mathrm{i}kx_0} - \frac{\rho\gamma^2}{K(\gamma, k)Z(0)}, \tag{3.16}$$

where the prime denotes partial derivative with respect to z. Substituting (3.15) and (3.16) into (3.5), we have

$$\begin{aligned}\tilde{G} = &-\frac{\mathrm{e}^{-\mathrm{i}kx_0}}{k}\frac{(Lk^4 + \rho g - m\gamma^2)k\cosh(kz_>) + \rho\gamma^2\sinh(kz_>)}{K(\gamma, k)Z(0)}Z(z_<) \\ &+ \frac{L}{2\pi}\frac{(\mathrm{i}k^3 A + k^2 B)[\cosh(kz_>) + \tanh(kH)\sinh(kz_>)]}{K(\gamma, k)Z(z_0)}Z(z_<).\end{aligned} \tag{3.17}$$

Using

$$\ln\left(\frac{r_1}{H}\right) = \int_0^{+\infty}\frac{\mathrm{e}^{-kH} - \mathrm{e}^{-k(z_> - z_<)}\cos[k(x - x_0)]}{k}\,\mathrm{d}k, \tag{3.18}$$

$$\ln\left(\frac{r_2}{H}\right) = \int_0^{+\infty}\frac{\mathrm{e}^{-kH} - \mathrm{e}^{-k(z_> + z_< + 2H)}\cos[k(x - x_0)]}{k}\,\mathrm{d}k, \tag{3.19}$$

https://doi.org/10.1017/jfm.2018.265 Published online by Cambridge University Press

where r_1 is the distance between p and q, and r_2 is the distance between p and the mirror image of q about the flat seabed $z=-H$, and then performing the inverse Fourier transform of $\tilde{G}$, the solution due to a single source can be written as

$$G = G_{ice}(x, z; x_0, z_0) + A \times \frac{\partial G_1(x, z)}{\partial x} + B \times G_1(x, z), \tag{3.20}$$

where

$$G_{ice} = \ln\left(\frac{r_1}{H}\right) + \ln\left(\frac{r_2}{H}\right) - 2\int_0^{+\infty} \frac{\mathrm{e}^{-kH}}{k}\{P(k)Z(z)Z(z_0)\cos[k(x-x_0)] + 1\}\,\mathrm{d}k, \tag{3.21}$$

with

$$P(k) = \frac{(Lk^4 + \rho g - m\gamma^2)k + \rho\gamma^2}{K(\gamma, k)Z(0)}, \tag{3.22}$$

and

$$G_1 = \frac{L}{\pi}\int_0^{+\infty} \frac{Z(z)}{K(\gamma, k)Z(0)} k^2 \cos(kx)\,\mathrm{d}k. \tag{3.23}$$

We may notice that G_{ice} is in fact the Green function without the crack (Evans & Porter 2003). We may also notice that G_1 satisfies (2.3) and

$$G_1(x, z) = \frac{L}{2\pi\rho\gamma^2}\left(\frac{\partial^3 G_{ice}(x_0, z_0; x, z)}{\partial z_0 \partial x_0^2}\right)_{x_0=0, z_0=0}. \tag{3.24}$$

For the current problem with a crack, there are still two unknown coefficients, A and B in (3.20), which can be determined by the condition in (2.4). The zero bending moment and shear force conditions respectively give

$$\lim_{x,z\to 0} G_{zxx} = \frac{2\pi\rho\gamma^2}{L} G_1(x_0, z_0) + A \lim_{x,z\to 0} \frac{\partial^4 G_1(x, z)}{\partial z \partial x^3} + B \lim_{x,z\to 0} \frac{\partial^3 G_1(x, z)}{\partial z \partial x^2} = 0, \tag{3.25}$$

$$\lim_{x,z\to 0} G_{zxxx} = -\frac{2\pi\rho\gamma^2}{L}\frac{\partial G_1(x_0, z_0)}{\partial x_0} + A \lim_{x,z\to 0} \frac{\partial^5 G_1(x, z)}{\partial z \partial x^4} + B \lim_{x,z\to 0} \frac{\partial^4 G_1(x, z)}{\partial z \partial x^3} = 0, \tag{3.26}$$

where (3.24) has been used. We then notice that when $x = r\sin\Theta$ and $z = -r\cos\Theta$ we have at $z<0$

$$\frac{\mathrm{e}^{\mathrm{i}(m+1)\Theta}}{r^{m+1}} = \frac{1}{m!}\int_0^{+\infty} \mathrm{e}^{kz} k^m \mathrm{e}^{\mathrm{i}kx}\,\mathrm{d}k. \tag{3.27}$$

This means that when $\Theta \to \pi/2$, or $z \to 0$, we have

$$\lim_{z\to 0}\int_0^{+\infty} \mathrm{e}^{kz} k^m \cos(kx)\,\mathrm{d}k = 0 \quad \text{for an even } m, \tag{3.28}$$

and

$$\lim_{z\to 0}\int_0^{+\infty} \mathrm{e}^{kz} k^m \sin(kx)\,\mathrm{d}k = 0 \quad \text{for an odd } m. \tag{3.29}$$

Equations (3.28) and (3.29) further provide

$$\lim_{z\to 0}\int_0^{+\infty} \frac{Z'(z)}{Z'(0)} k^m \cos(kx)\,\mathrm{d}k = 0 \quad \text{for an even } m, \tag{3.30}$$

https://doi.org/10.1017/jfm.2018.265 Published online by Cambridge University Press

and

$$\lim_{z\to 0}\int_0^{+\infty}\frac{Z'(z)}{Z'(0)}k^m\sin(kx)\,\mathrm{d}k=0\quad\text{for an odd } m. \tag{3.31}$$

Using these two equations, we have

$$\lim_{z\to 0}\frac{\partial^3 G_1(x,z)}{\partial z\partial x^2}=-\frac{1}{\pi}\int_0^{+\infty}\frac{\rho\gamma^2-(\rho g-m\gamma^2)k\tanh(kH)}{K(\gamma,k)}\cos(kx)\,\mathrm{d}k, \tag{3.32}$$

$$\lim_{z\to 0}\frac{\partial^4 G_1(x,z)}{\partial z\partial x^3}=\frac{1}{\pi}\int_0^{+\infty}\frac{\rho\gamma^2-(\rho g-m\gamma^2)k\tanh(kH)}{K(\gamma,k)}k\sin(kx)\,\mathrm{d}k, \tag{3.33}$$

$$\lim_{z\to 0}\frac{\partial^5 G_1(x,z)}{\partial z\partial x^4}=\frac{1}{\pi}\int_0^{+\infty}\frac{\rho\gamma^2-(\rho g-m\gamma^2)k\tanh(kH)}{K(\gamma,k)}k^2\cos(kx)\,\mathrm{d}k. \tag{3.34}$$

Through these results, (3.26) and (3.25) then respectively give

$$A=\frac{2\pi^2\rho\gamma^2}{L\mathcal{I}_1}\frac{\partial G_1(x_0,z_0)}{\partial x_0}, \tag{3.35}$$

and

$$B=\frac{2\pi^2\rho\gamma^2}{L\mathcal{I}_2}G_1(x_0,z_0), \tag{3.36}$$

where

$$\mathcal{I}_1=\pi\lim_{x,z\to 0}\frac{\partial^5 G_1(x,z)}{\partial z\partial x^4}=\int_0^{+\infty}\frac{\rho\gamma^2-(\rho g-m\gamma^2)k\tanh(kH)}{K(\gamma,k)}k^2\,\mathrm{d}k, \tag{3.37a}$$

$$\mathcal{I}_2=-\pi\lim_{x,z\to 0}\frac{\partial^3 G_1(x,z)}{\partial z\partial x^2}=\int_0^{+\infty}\frac{\rho\gamma^2-(\rho g-m\gamma^2)k\tanh(kH)}{K(\gamma,k)}\,\mathrm{d}k. \tag{3.37b}$$

Substituting (3.35) and (3.36) into (3.20), we then obtain the solution of the Green function for an ice sheet with a crack at the origin

$$G=G_{ice}(x,z;x_0,z_0)+\frac{2\pi^2\rho\gamma^2}{L}\left[\frac{1}{\mathcal{I}_1}\frac{\partial G_1(x,z)}{\partial x}\frac{\partial G_1(x_0,z_0)}{\partial x_0}+\frac{G_1(x,z)G_1(x_0,z_0)}{\mathcal{I}_2}\right]. \tag{3.38}$$

The replacement of ω with $\gamma=\omega-\mathrm{i}\epsilon$ in (2.8) during the derivation moves the pole $k=\lambda$ off the real axis of k. Letting $\epsilon\to 0^+$, the Taylor expansion of the dispersion equation $K(\gamma,k)$ with respect to ϵ provides the root at

$$k=\lambda-\mathrm{i}\epsilon', \tag{3.39}$$

where

$$\epsilon'=\frac{\epsilon}{\omega}\frac{L\lambda^4+\rho g}{L\lambda^4+\rho g-m\omega^2}\Big/\left[\frac{1}{2\lambda}+\frac{H}{\sinh(2\lambda H)}+\frac{2L\lambda^3}{L\lambda^4+\rho g-m\omega^2}\right]. \tag{3.40}$$

Thus when $\epsilon\to 0^+$, the pole will approach the real axis of k from below. Therefore, the integration route $\mathcal{D}$ in (3.38) from 0 to $+\infty$ should pass over the pole at $k=\lambda$, which is consistent with the radiation condition, i.e. the wave will propagate away from the source into infinity. With such a definition of $\mathcal{D}$, γ in (3.38) can be replaced by ω. We may notice that (3.38) is a summation of the Green function G_{ice} for the

https://doi.org/10.1017/jfm.2018.265 Published online by Cambridge University Press

ice sheet without the crack and two additional terms equivalent to the loads applied at the crack to ensure that the shear force and bending moment there are zero. We may also notice that the integrand of G in (3.38) has only a simple pole at $k=\lambda$ where $K(\omega, k)=0$. The integration may be calculated by using the Gauss–Legendre principal value integration procedure (Noble 2000). This may also be done by following the numerical procedure in Wu & Eatock Taylor (1987), which effectively removes the singularity.

3.2. *Multipole expansion*

Potentials due to multipoles or singularities of higher order may be found by differentiating (3.38) with respect to the position of the source point. In such a way, none of the boundary conditions will be affected and will be still satisfied. As shown in figure 1, we have $x-x_0=r\sin\theta$ and $z-z_0=r\cos\theta$. Similar to Wu (1998), we may apply the operator

$$(D_\pm)^n=-\frac{1}{2^{n-1}(n-1)!}\left(\frac{\partial}{\partial z_0}\pm \mathrm{i}\frac{\partial}{\partial x_0}\right)^n \tag{3.41}$$

to (3.38). Using the result

$$(D_\pm)^n \ln(r_1)=\frac{\mathrm{e}^{\pm \mathrm{i}n\theta}}{r^n}, \tag{3.42}$$

and noticing $(D_+)\exp(\pm kz_0\pm \mathrm{i}kx_0)=0$ and $(D_-)\exp(\pm kz_0\mp \mathrm{i}kx_0)=0$, we have

$$\begin{aligned} f_n &= (D_+)^n G \\ &= \frac{\mathrm{e}^{+\mathrm{i}n\theta}}{r^n}+\frac{(-1)^n}{(n-1)!}\int_0^{+\infty}\mathrm{e}^{-k(z+z_0+2H)-\mathrm{i}k(x-x_0)}k^{n-1}\,\mathrm{d}k \\ &\quad +\frac{2\mathrm{i}^n}{(n-1)!}\int_{\mathcal{D}} Z(z)\cosh[k(z_0+H)+\mathrm{i}k(x-x_0)-\mathrm{i}n\pi/2]\mathrm{e}^{-kH}P(k)k^{n-1}\,\mathrm{d}k \\ &\quad -\frac{\pi\rho\omega^2}{(n-1)!}\left[\frac{\mathrm{i}\mathcal{G}_1(n)}{\mathcal{I}_1}\frac{\partial G_1(x,z)}{\partial x}-\frac{\mathcal{G}_1(n-1)G_1(x,z)}{\mathcal{I}_2}\right], \end{aligned} \tag{3.43}$$

and

$$\begin{aligned} g_n &= (D_-)^n G \\ &= \frac{\mathrm{e}^{-\mathrm{i}n\theta}}{r^n}+\frac{(-1)^n}{(n-1)!}\int_0^{+\infty}\mathrm{e}^{-k(z+z_0+2H)+\mathrm{i}k(x-x_0)}k^{n-1}\,\mathrm{d}k \\ &\quad +\frac{2\mathrm{i}^n}{(n-1)!}\int_{\mathcal{D}} Z(z)\cosh[k(z_0+H)-\mathrm{i}k(x-x_0)-\mathrm{i}n\pi/2]\mathrm{e}^{-kH}P(k)k^{n-1}\,\mathrm{d}k \\ &\quad +\frac{\pi\rho\omega^2}{(n-1)!}\left[\frac{\mathrm{i}\mathcal{G}_2(n)}{\mathcal{I}_1}\frac{\partial G_1(x,z)}{\partial x}+\frac{\mathcal{G}_2(n-1)G_1(x,z)}{\mathcal{I}_2}\right], \end{aligned} \tag{3.44}$$

where

$$\mathcal{G}_1(n)=\int_{\mathcal{D}}\frac{(-1)^n\mathrm{e}^{-k(z_0+H)+\mathrm{i}kx_0}-\mathrm{e}^{k(z_0+H)-\mathrm{i}kx_0}}{K(\omega,k)Z(0)}k^{n+3}\,\mathrm{d}k, \tag{3.45a}$$

$$\mathcal{G}_2(n)=\int_{\mathcal{D}}\frac{(-1)^n\mathrm{e}^{-k(z_0+H)-\mathrm{i}kx_0}-\mathrm{e}^{k(z_0+H)+\mathrm{i}kx_0}}{K(\omega,k)Z(0)}k^{n+3}\,\mathrm{d}k. \tag{3.45b}$$

We notice here that when i in (3.43) is replaced by $-\mathrm{i}$, f_n becomes g_n.

https://doi.org/10.1017/jfm.2018.265 Published online by Cambridge University Press

3.3. *Solution for the radiation problem*

Here we consider the wave radiation due to the body undergoing sinusoidal oscillation with frequency ω. By using (3.43) and (3.44), we can write the potentials ϕ_j in terms of multipole expansions in the polar coordinate system as

$$\phi_j = \sum_{n=1}^{\infty} a^n (A_n^j f_n + B_n^j g_n). \tag{3.46}$$

ϕ_j now satisfies the governing equation and all the boundary conditions apart from that on the body surface, which is to be used to obtain the coefficients A_n^j and B_n^j. When $j = 1, 2$, we respectively have

$$\frac{\partial \phi_1}{\partial r} = -\frac{\partial \phi_1}{\partial n} = \sin\theta \quad \text{and} \quad \frac{\partial \phi_2}{\partial r} = -\frac{\partial \phi_2}{\partial n} = \cos\theta, \quad (r = a), \tag{3.47a,b}$$

where the minus sign is due to the fact that $\boldsymbol{n}$ points into the body. Since

$$\mathrm{e}^{kz \pm \mathrm{i}kx} = \exp(kz_0 \pm \mathrm{i}kx_0 + kr\mathrm{e}^{\pm \mathrm{i}\theta}) = \mathrm{e}^{kz_0 \pm \mathrm{i}kx_0} \sum_{l=0}^{\infty} \frac{k^l r^l \mathrm{e}^{\pm \mathrm{i}l\theta}}{l!}, \tag{3.48}$$

ϕ_j can be expressed in the polar coordinate system as

$$\begin{aligned} \phi_j = & \sum_{n=1}^{\infty} A_n^j a^n \left\{ \frac{\mathrm{e}^{+\mathrm{i}n\theta}}{r^n} + \frac{1}{(n-1)!} \sum_{l=0}^{\infty} \frac{r^l}{l!} [\mathrm{e}^{+\mathrm{i}l\theta} C(n, l) + \mathrm{e}^{-\mathrm{i}l\theta} D(n, l)] \right\} \\ & + \sum_{n=1}^{\infty} B_n^j a^n \left\{ \frac{\mathrm{e}^{-\mathrm{i}n\theta}}{r^n} + \frac{1}{(n-1)!} \sum_{l=0}^{\infty} \frac{r^l}{l!} [\mathrm{e}^{-\mathrm{i}l\theta} C(l, n) + \mathrm{e}^{+\mathrm{i}l\theta} E(n, l)] \right\}, \end{aligned} \tag{3.49}$$

where

$$C(n, l) = (-1)^{n+l} \mathcal{J}_1(n + l) + \frac{\mathcal{J}_3(n + l)}{2} - \frac{L\rho\omega^2}{4} \left[\frac{\mathcal{G}_1(n)\mathcal{G}_2(l)}{\mathcal{I}_1} + \frac{\mathcal{G}_1(n-1)\mathcal{G}_2(l-1)}{\mathcal{I}_2} \right], \tag{3.50a}$$

$$D(n, l) = [(-1)^l + (-1)^n] \frac{\mathcal{J}_2(n + l)}{2} + \frac{L\rho\omega^2}{4} \left[\frac{\mathcal{G}_1(n)\mathcal{G}_1(l)}{\mathcal{I}_1} - \frac{\mathcal{G}_1(n-1)\mathcal{G}_1(l-1)}{\mathcal{I}_2} \right], \tag{3.50b}$$

$$E(n, l) = [(-1)^l + (-1)^n] \frac{\mathcal{J}_2(n + l)}{2} + \frac{L\rho\omega^2}{4} \left[\frac{\mathcal{G}_2(n)\mathcal{G}_2(l)}{\mathcal{I}_1} - \frac{\mathcal{G}_2(n-1)\mathcal{G}_2(l-1)}{\mathcal{I}_2} \right], \tag{3.50c}$$

and

$$\mathcal{J}_1(n) = \Gamma(n)/[2(z_0 + H)]^n, \tag{3.51a}$$

$$\mathcal{J}_2(n) = \int_{\mathcal{D}} \mathrm{e}^{-kH} P(k) k^{n-1} \, \mathrm{d}k, \tag{3.51b}$$

$$\mathcal{J}_3(n) = \int_{\mathcal{D}} [(-1)^n \mathrm{e}^{-2k(z_0+H)} + \mathrm{e}^{2k(z_0+H)}] \mathrm{e}^{-kH} P(k) k^{n-1} \, \mathrm{d}k. \tag{3.51c}$$

https://doi.org/10.1017/jfm.2018.265 Published online by Cambridge University Press

Here, $\Gamma(n)$ is the gamma function (Abramowitz & Stegun 1965). Invoking (3.47), then using the orthogonality of trigonometric function, we have

$$-l\frac{A_l^j}{a}+\sum_{n=1}^{\infty}\frac{A_n^j a^{n+l-1}C(n,l)}{(n-1)!(l-1)!}+\sum_{n=1}^{\infty}\frac{B_n^j a^{n+l-1}E(n,l)}{(n-1)!(l-1)!}=u_l(j), \tag{3.52}$$

and

$$-l\frac{B_l^j}{a}+\sum_{n=1}^{\infty}\frac{B_n^j a^{n+l-1}C(l,n)}{(n-1)!(l-1)!}+\sum_{n=1}^{\infty}\frac{A_n^j a^{n+l-1}D(n,l)}{(n-1)!(l-1)!}=v_l(j), \tag{3.53}$$

for $l=1,2,\ldots,$ where

$$u_l(1)=\tfrac{1}{2\mathrm{i}}\delta_{l1},\quad v_l(1)=-u_l(1), \tag{3.54a,b}$$

and

$$u_l(2)=\tfrac{1}{2}\delta_{l1},\quad v_l(2)=u_l(2). \tag{3.55a,b}$$

Here δ_{l1} is the Kronecker delta function, and $j=1,2$ in (3.52) and (3.53) correspond to ϕ_1 and ϕ_2 respectively. For each l, (3.52) and (3.53) provide two linear equations for A_n^j and B_n^j. Thus when the infinite summation is truncated at a finite number, we can obtain a matrix equation, from which A_n^j and B_n^j can be solved. When the solutions for ϕ_1 and ϕ_2 have been obtained, the added mass μ_{js} and damping coefficients λ_{js} can be computed through (Newman 1977)

$$\tau_{js}=\mu_{js}-\mathrm{i}\frac{\lambda_{js}}{\omega}=\rho\int_{S_0}\phi_s n_j\,\mathrm{d}S, \tag{3.56}$$

for $j,s=1,2$, where S_0 represents the body surface. Multiplying both sides of (3.52) and (3.53) respectively by $\mathrm{e}^{+\mathrm{i}l\theta}$ and $\mathrm{e}^{-\mathrm{i}l\theta}$, then taking summation with respect to l from 1 to $+\infty$, substituting the obtained results into (3.49), and letting $r=a$, we have (Wu 1993)

$$\phi_s=2\sum_{n=1}^{\infty}[A_n^s\mathrm{e}^{+\mathrm{i}n\theta}+B_n^s\mathrm{e}^{-\mathrm{i}n\theta}]+a\sum_{n=1}^{\infty}\frac{1}{n}[\mathrm{e}^{+\mathrm{i}n\theta}u_n(s)+\mathrm{e}^{-\mathrm{i}n\theta}v_n(s)]+\phi_c^s, \tag{3.57}$$

where

$$\phi_c^s=\sum_{n=1}^{\infty}\frac{A_n^s a^n}{(n-1)!}[C(n,0)+D(n,0)]+\sum_{n=1}^{\infty}\frac{B_n^s a^n}{(n-1)!}[C(0,n)+E(n,0)]. \tag{3.58}$$

Substituting (3.57) into (3.56), we obtain

$$\tau_{1s}=-\mathrm{i}2\pi\rho a(A_1^s-B_1^s)-\delta_{1s}\pi\rho a^2, \tag{3.59}$$

and

$$\tau_{2s}=-2\pi\rho a(A_1^s+B_1^s)-\delta_{2s}\pi\rho a^2. \tag{3.60}$$

https://doi.org/10.1017/jfm.2018.265 Published online by Cambridge University Press

3.4. *Solution for the diffraction problem*

Wave diffraction potential consists of two parts and the total diffraction potential ϕ_D can be written as

$$\phi_D = \phi_D^1 + \phi_D^2, \tag{3.61}$$

where ϕ_D^1 is the diffraction potential by the crack to ϕ_I, and ϕ_D^2 is the diffraction potential by the cylinder to $\varphi = \phi_I + \phi_D^1$. For a periodic wave from $x = -\infty$ to $x = +\infty$, ϕ_I can be given as

$$\phi_I = I\mathrm{e}^{-\mathrm{i}\lambda x}\psi(z), \tag{3.62}$$

with

$$\psi(z) = \cosh[\lambda(H+z)]/\cosh(\lambda H), \tag{3.63}$$

and $I = g/\mathrm{i}\omega$. Applying the Green's second identity to ϕ_D^1 and G in (3.38) over the fluid boundary S, we have

$$2\pi\phi_D^1(x,z) = \int_S \left[\phi_D^1(\xi,\zeta)\frac{\partial G(x,z;\xi,\zeta)}{\partial n} - G(x,z;\xi,\zeta)\frac{\partial \phi_D^1(\xi,\zeta)}{\partial n}\right] \mathrm{d}S, \tag{3.64}$$

where the derivative and integration are with respect to (ξ,ζ). Invoking the boundary conditions for ϕ_D^1 and G, only the ice sheet will remain on the right-hand side of (3.64). Using condition (2.3) and through integrating by parts, this equation can be further written as

$$2\pi\phi_D^1 = \frac{L}{\rho\omega^2}\left[\left(\frac{\partial^4\phi_D^1}{\partial\xi^3\partial\zeta}\frac{\partial G}{\partial\zeta} - \frac{\partial^3\phi_D^1}{\partial\xi^2\partial\zeta}\frac{\partial^2 G}{\partial\xi\,\partial\zeta}\right)_{\xi=0^+}^{\xi=0^-}\right]_{\zeta=0}. \tag{3.65}$$

Noticing that $\varphi = \phi_I + \phi_D^1$ should satisfy the crack condition in (2.4), then $\phi_D^1(x,z)$ can be obtained directly through the Green function as

$$\phi_D^1 = -\pi I\lambda^3\tanh(\lambda H)\left[\frac{\mathrm{i}\lambda}{\mathcal{I}_1}\frac{\partial G_1(x,z)}{\partial x} + \frac{G_1(x,z)}{\mathcal{I}_2}\right]. \tag{3.66}$$

To obtain the solution for ϕ_D^2, $\varphi = \phi_I + \phi_D^1$ can be expressed in the polar coordinate system through using (3.48)

$$\varphi = I\sum_{n=0}^{\infty}\frac{r^n}{4n!}[\mathrm{e}^{+\mathrm{i}n\theta}\mathcal{F}_1(n) + \mathrm{e}^{-\mathrm{i}n\theta}\mathcal{F}_2(n)], \tag{3.67}$$

where

$$\mathcal{F}_1(n) = \frac{2(-\lambda)^n\mathrm{e}^{-\lambda(z_0+H)-\mathrm{i}\lambda x_0}}{\cosh(\lambda H)} - L\lambda^3\tanh(\lambda H)\left[\frac{\lambda\mathcal{G}_2(n)}{\mathcal{I}_1} - \frac{\mathcal{G}_2(n-1)}{\mathcal{I}_2}\right], \tag{3.68a}$$

$$\mathcal{F}_2(n) = \frac{2\lambda^n\mathrm{e}^{\lambda(z_0+H)-\mathrm{i}\lambda x_0}}{\cosh(\lambda H)} + L\lambda^3\tanh(\lambda H)\left[\frac{\lambda\mathcal{G}_1(n)}{\mathcal{I}_1} + \frac{\mathcal{G}_1(n-1)}{\mathcal{I}_2}\right]. \tag{3.68b}$$

Then invoking the boundary condition on the body surface for ϕ_D^2

$$\frac{\partial\phi_D^2}{\partial n} = -\frac{\partial\varphi}{\partial n}, \tag{3.69}$$

https://doi.org/10.1017/jfm.2018.265 Published online by Cambridge University Press

we have

$$u_l(0) = -\frac{Ia^{l-1}\mathcal{F}_1(l)}{4(l-1)!}, \quad v_l(0) = -\frac{Ia^{l-1}\mathcal{F}_2(l)}{4(l-1)!}, \tag{3.70a,b}$$

for $j=0$ in (3.52) and (3.53) respectively. Invoking (3.57) we further have at $r=a$

$$\phi_D^2 = 2\sum_{n=1}^{\infty}[A_n^0 \mathrm{e}^{+\mathrm{i}n\theta} + B_n^0 \mathrm{e}^{-\mathrm{i}n\theta}] + a\sum_{n=1}^{\infty}\frac{1}{n}[\mathrm{e}^{+\mathrm{i}n\theta}u_n(0) + \mathrm{e}^{-\mathrm{i}n\theta}v_n(0)] + \phi_c^0. \tag{3.71}$$

When the solution for ϕ_D^2 has been obtained, the wave exciting force can be computed through (Newman 1977)

$$f_{E,j} = -\mathrm{i}\omega\rho\int_{S_0}\phi_0 n_j\,\mathrm{d}S. \tag{3.72}$$

Substituting (3.71) together with (3.67) into (3.72), we have

$$f_{E,1} = -2\pi a\rho\omega(A_1^0 - B_1^0), \tag{3.73}$$

$$f_{E,2} = \mathrm{i}2\pi a\rho\omega(A_1^0 + B_1^0). \tag{3.74}$$

We may notice that $f_{E,j}$ in (3.72) can be also computed through φ and ϕ_j by using the Haskind relation (C 5).

3.5. *Some special cases*

3.5.1. *Simplified solution procedure at large* $|x_0/a|$

When the circular cylinder is located far away from the crack, or $|x_0/a| \gg 1$, the problems in §§ 3.3 and 3.4 can be solved by using the wide spacing approximation, based on the assumption that the mutual effects of evanescent waves between the crack and the body can be neglected. Without losing generality, here we may assume $x_0 > 0$ and the incoming wave is from $x=-\infty$. We denote the radiation and scattering potentials of the body, with its centre at $x=0$ and submerged below the ice sheet without the crack, as ψ_j^r and ψ_0 respectively. The solutions of these potentials can be obtained by dropping the terms of $\mathcal{I}_1$ and $\mathcal{I}_2$ in (3.43) and (3.44), and the procedure will be much simpler. We further define the velocity potentials ψ_L and ψ_R for ice sheet with a crack but without the body. They correspond to incoming waves from $x=-\infty$ and $x=+\infty$ respectively, and contain both the incident and diffracted potentials. These two potentials can be obtained directly from (3.62) and (3.66). Using these results the solution for the current problem of a body submerged beneath an ice sheet with a crack can be easily constructed for $|x_0/a| \gg 1$, following the method used for multiple bodies with a large gap (Srokosz & Evans 1979) and a floating body in a wide polynya (Li *et al.* 2017*a*).

We may notice that the transmission coefficient T_c and reflection coefficient R_c corresponding to ψ_L and ψ_R are the same, which can be easily confirmed through reversing the direction of the x axis. At infinity, the evanescent waves will tend to zero and the velocity potentials defined above will have the following asymptotic forms

$$\psi_j^r = A_j^{\pm}\mathrm{e}^{\mp\mathrm{i}\lambda x}\psi(z) \text{ as } x\to\pm\infty, \quad (j=1,2), \tag{3.75a}$$

$$\psi_0 = t_0\mathrm{e}^{-\mathrm{i}\lambda x}\psi(z) \text{ as } x\to+\infty, \tag{3.75b}$$

https://doi.org/10.1017/jfm.2018.265 Published online by Cambridge University Press

$$\psi_0 = (\mathrm{e}^{-\mathrm{i}\lambda x} + r_0 \mathrm{e}^{+\mathrm{i}\lambda x})\psi(z) \text{ as } x \to -\infty, \tag{3.75c}$$

$$\psi_L = T_c \mathrm{e}^{-\mathrm{i}\lambda x}\psi(z) \text{ as } x \to +\infty, \tag{3.75d}$$

$$\psi_L = (\mathrm{e}^{-\mathrm{i}\lambda x} + R_c \mathrm{e}^{+\mathrm{i}\lambda x})\psi(z) \text{ as } x \to -\infty, \tag{3.75e}$$

$$\psi_R = (\mathrm{e}^{+\mathrm{i}\lambda x} + R_c \mathrm{e}^{-\mathrm{i}\lambda x})\psi(z) \text{ as } x \to +\infty, \tag{3.75f}$$

$$\psi_R = T_c \mathrm{e}^{+\mathrm{i}\lambda x}\psi(z) \text{ as } x \to -\infty. \tag{3.75g}$$

For the submerged circular cylinder undergoing oscillation in the jth mode, by following the procedure in Srokosz & Evans (1979), the velocity potential near the body can be written as a summation of the potential without a crack and the potential due to the wave reflected by the crack

$$\phi_j(x, z) = \psi_j^r(x - x_0, z) + \epsilon_j \psi_0(x - x_0, z). \tag{3.76}$$

Near the crack we may write the velocity potential as

$$\phi_j(x, z) = \eta_j \psi_R(x, z), \tag{3.77}$$

which is due to the incoming wave to the crack generated by the body motion and its reflection by the crack. ϵ_j and η_j in the two equations are two unknown coefficients to be determined. $x - x_0$ in (3.76) reflects the fact that the solutions for ψ_j^r and ψ_0 correspond to the cylinder with centre located at $(0, z_0)$, which in the current problem is at (x_0, z_0).

The solution has now been constructed based on results which could be obtained much more easily. The only task is to find the two unknown coefficients. We may consider (3.76) and (3.77) at a vertical line at $x = x_I$ between the crack and cylinder. On this vertical interface, the continuity conditions of pressure and normal velocity may be enforced, i.e.

$$\phi_j(x_{I-}, z) = \phi_j(x_{I+}, z), \quad \frac{\partial \phi_j(x_{I-}, z)}{\partial x} = \frac{\partial \phi_j(x_{I+}, z)}{\partial x}, \tag{3.78a,b}$$

where the subscripts $+$ and $-$ mean that the potentials should be taken from the solutions on the right- and left-hand sides of the vertical line, or (3.76) and (3.77), respectively. On the basis $0 \ll x_I \ll x_0$, (3.75a)–(3.75g) become applicable at $x = x_I$. Substituting (3.76) and (3.77), and the corresponding asymptotic expansions into (3.78), we can obtain

$$\epsilon_j = \frac{A_j^- R_c}{\mathrm{e}^{2\mathrm{i}\lambda x_0} - R_c r_0}, \tag{3.79}$$

$$\eta_j = \frac{A_j^- \mathrm{e}^{\mathrm{i}\lambda x_0}}{\mathrm{e}^{2\mathrm{i}\lambda x_0} - R_c r_0}. \tag{3.80}$$

Substituting (3.76) into (3.56), we can obtain the added mass and damping coefficient as

$$\tau_{js} = \tau_{js}^o - \epsilon_s f_{E,j}^o / g, \tag{3.81}$$

where the superscript o means that the results are from the ice sheet without crack.

Similarly, for the diffraction problem, near the body we may write the potential as

$$\phi_0(x, z) = \epsilon_0 \psi_0(x - x_0, z), \tag{3.82}$$

https://doi.org/10.1017/jfm.2018.265 Published online by Cambridge University Press

and near the crack we may write the potential as

$$\phi_0(x, z) = \psi_L(x, z) + \eta_0 \psi_R(x, z). \tag{3.83}$$

Using the asymptotic expansion and imposing the continuity condition (3.78) at $x = x_I$, we have

$$\epsilon_0 = \frac{T_c e^{i\lambda x_0}}{e^{2i\lambda x_0} - R_c r_0}, \tag{3.84}$$

$$\eta_0 = \frac{T_c r_0}{e^{2i\lambda x_0} - R_c r_0}. \tag{3.85}$$

Substituting (3.82) into (3.72), we can obtain the wave exciting force on the cylinder below the ice sheet with a crack from the result without the crack

$$f_{E,j} = \epsilon_0 f^o_{E,j}. \tag{3.86}$$

We should notice that (3.81) and (3.86) are not limited to a circular cylinder and they are applicable for a body of arbitrary shape.

3.5.2. *Solution for infinite water depth*

When the water depth tends to infinity or $H \to +\infty$, G_{ice} and G_1 in the Green function (3.38) respectively become

$$G_{ice} = \ln(r_1) - \ln(r_1') - 2\int_{\mathcal{D}} \frac{Lk^4 + \rho g - m\omega^2}{K(\omega, k)} e^{k(z+z_0)} \cos[k(x - x_0)]\, dk, \tag{3.87}$$

and

$$G_1 = \frac{L}{\pi} \int_{\mathcal{D}} \frac{e^{kz}}{K(\omega, k)} k^2 \cos(kx)\, dk, \tag{3.88}$$

together with $\mathcal{I}_1$ and $\mathcal{I}_2$ simplified as

$$\mathcal{I}_1 = \int_{\mathcal{D}} \frac{\rho\omega^2 - (\rho g - m\omega^2)k}{K(\omega, k)} k^2\, dk, \tag{3.89a}$$

$$\mathcal{I}_2 = \int_{\mathcal{D}} \frac{\rho\omega^2 - (\rho g - m\omega^2)k}{K(\omega, k)}\, dk, \tag{3.89b}$$

where r_1' is the distance between p and the mirror image of q about the mean upper surface $z = 0$, and

$$K(\omega, k) = (Lk^4 + \rho g - m\omega^2)k - \rho\omega^2. \tag{3.90}$$

For the multipole expansions, (3.45*a*) and (3.45*b*) become

$$\mathcal{G}_1(n) = -2\int_{\mathcal{D}} \frac{e^{kz_0 - ikx_0}}{K(\omega, k)} k^{n+3}\, dk, \tag{3.91a}$$

$$\mathcal{G}_2(n) = -2\int_{\mathcal{D}} \frac{e^{kz_0 + ikx_0}}{K(\omega, k)} k^{n+3}\, dk, \tag{3.91b}$$

https://doi.org/10.1017/jfm.2018.265 Published online by Cambridge University Press

and (3.51*a*)–(3.51*c*) are simplified as

$$\mathcal{J}_1(n) = 0, \tag{3.92a}$$

$$\mathcal{J}_2(n) = 0, \tag{3.92b}$$

$$\mathcal{J}_3(n) = 2\int_{\mathcal{D}} \left[1 + \frac{2\rho\omega^2}{K(\omega, k)}\right] \mathrm{e}^{2kz_0} k^{n-1}\, \mathrm{d}k. \tag{3.92c}$$

For the problem of wave propagation across the crack, $\mathcal{F}_1(n)$ and $\mathcal{F}_2(n)$ in (3.67) respectively become

$$\mathcal{F}_1(n) = -L\lambda^3 \left[\frac{\lambda \mathcal{G}_2(n)}{\mathcal{I}_1} - \frac{\mathcal{G}_2(n-1)}{\mathcal{I}_2}\right], \tag{3.93a}$$

$$\mathcal{F}_2(n) = 4\lambda^4 \mathrm{e}^{\lambda z_0 - \mathrm{i}\lambda x_0} + L\lambda^3 \left[\frac{\lambda \mathcal{G}_1(n)}{\mathcal{I}_1} + \frac{\mathcal{G}_1(n-1)}{\mathcal{I}_2}\right]. \tag{3.93b}$$

The simplified solution in § 3.5.1 can be also extended to infinite water depth. This is obtained by setting $\psi(z)$ in (3.75*a–g*) as $\mathrm{e}^{\lambda z}$, while the other equations remain the same.

When there is no ice crack, i.e. removing the terms $\mathcal{I}_1$ and $\mathcal{I}_2$, $\mathcal{F}_1(n)$ in (3.93*a*) and $E(n, l)$ in (3.50*c*) become zero. Then (3.52) provides $A_l^0 = 0$. By letting $H \to +\infty$ in (3.44), we obtain $\lim_{x\to-\infty} g_n = 0$. Thus according to (3.46), we can conclude that there is no wave reflection by the circular cylinder. If the ice thickness is taken to be zero, this becomes the well-known case for a free surface, as has been shown by Dean (1948) and Ursell (1950). When the ice sheet has a crack, this conclusion is not true in general. However (3.91*b*) provides $\lim_{x_0\to+\infty} \mathcal{G}_2(n) = 0$ and we can also obtain $A_l^0 = 0$. Thus there will be no reflection in such a case. This is of course quite obvious as the wave due to $\varphi = \phi_I + \phi_D^1$ becomes the normal incident wave when $x_0 \to +\infty$, or the cylinder is infinitely far away from the crack.

4. Numerical results

The typical physical parameters of the ice sheet are chosen to be the same as those in Sturova (2015*b*), i.e.

$$E = 5\ \text{Gpa}, \quad \nu = 0.3, \quad \rho_0 = 922.5\ \text{kg m}^{-3}, \quad \rho = 1025\ \text{kg m}^{-3}, \quad H = 100\ \text{m}. \tag{4.1a–e}$$

Numerical results are obtained by truncating the infinite series of the multipole expansions at a finite number $n = N$, and they are presented in the dimensionless form, based on a characteristic length scale, the density of water ρ and acceleration due to gravity $g = 9.80\ \text{m s}^{-2}$.

4.1. *Wave scattering by an ice crack*

We may use the problem of wave propagation beneath an ice sheet with a crack to first verify the present formulation. The case has been considered by Evans & Porter (2003). In that work, the problem was first divided into the symmetric and antisymmetric parts, and then Green's identity was applied to each part together with the Green function satisfying the condition on the ice sheet without a crack. Thus the result for each part turned out to be a single series multiplied by an unknown constant which was further determined by the condition at the crack. Here, by taking

https://doi.org/10.1017/jfm.2018.265 Published online by Cambridge University Press

the advantage of the Green function in (3.38), which itself already satisfies the ice crack condition, the solution can be obtained directly through the Green identity, as shown in (3.66). If we convert the integration in (3.66) into series form, it can be found that the solution is identical to that of Evans & Porter (2003). Taking $x \leqslant 0$ as an example, we first extend the route of integrations in (3.66) to $k \in (-\infty, +\infty)$, and add an integration along a semicircle of infinite radius in the lower half-complex plane of k. The latter does not affect the result as it is in fact a zero term, which follows Jordan's lemma. Then using residue theorem and noticing the poles at $-k_n$, $n = -2, -1, 0, 1, \ldots$ in the lower half-plane, the potential φ can be expressed in the series form as

$$\varphi = \frac{I}{Z_0(0)}\varphi_0, \tag{4.2}$$

where

$$\begin{aligned}\varphi_0 \;=\; & \mathrm{e}^{\mathrm{i}k_0 x} Z_0(z) \\ & + \left[\frac{k_0^3 Z_0'(0)}{\displaystyle\sum_{n=-2}^{\infty} \frac{k_n^6 Z_n'(0)}{\mathcal{X}'(k_n)}} \sum_{n=-2}^{\infty} \frac{k_n^3 Z_n(z)\mathrm{e}^{-\mathrm{i}k_n x}}{\mathcal{X}'(k_n)} - \frac{k_0^2 Z_0'(0)}{\displaystyle\sum_{n=-2}^{\infty} \frac{k_n^4 Z_n'(0)}{\mathcal{X}'(k_n)}} \sum_{n=-2}^{\infty} \frac{k_n^2 Z_n(z)\mathrm{e}^{-\mathrm{i}k_n x}}{\mathcal{X}'(k_n)} \right],\end{aligned} \tag{4.3}$$

and

$$\mathcal{X}(k) = (L\lambda^4 + \rho g - m\omega^2)k \sinh(kH) - \rho\omega^2 \cosh(kH), \tag{4.4}$$

$$Z_n(z) = \cosh[k_n(z + H)]. \tag{4.5}$$

Here, $k_0 = -\lambda$, k_n with $n = 1, 2, \ldots$ are the purely positive imaginary roots of (2.8), k_{-1} and k_{-2} are the corresponding two complex roots with positive imaginary parts. It can be seen that (4.3) is identical to (2.17) in Evans & Porter (2003) for the normal incident case, by noticing that the time factor adopted by them is $\mathrm{e}^{-\mathrm{i}\omega t}$, while $\mathrm{e}^{+\mathrm{i}\omega t}$ is used in (2.1) here.

At $x \to \pm\infty$, by applying the Fourier integrals (13.16) in Wehausen & Laitone (1960) to ϕ_D^1 in (3.66), the potential φ can be given as

$$\varphi = \begin{cases} I \times T_c \mathrm{e}^{-\mathrm{i}\lambda x}\psi(z) & \text{at } x \to +\infty \\ I(\mathrm{e}^{-\mathrm{i}\lambda x} + R_c \mathrm{e}^{+\mathrm{i}\lambda x})\psi(z) & \text{at } x \to -\infty, \end{cases} \tag{4.6}$$

with transmission coefficient T_c and reflection coefficient R_c given in (B 7) and (B 8) respectively. It may be interesting to compare these results for wave propagation below an ice sheet with a crack and those through a polynya confined between two semi-infinite ice sheets. When the polynya width b tends to zero, the result is expected to tend to that of an ice sheet with a crack. Comparison of the reflection coefficients is shown in figure 2, where $\sigma = \omega^2 h/g$, and $|R_p|$ for polynya with $b = 0.05$ is computed by MEE (Ren *et al.* 2016). From the figure, it can be seen that $|R_p|$ and $|R_c|$ agree with each other very well within the frequency range calculated.

https://doi.org/10.1017/jfm.2018.265 Published online by Cambridge University Press

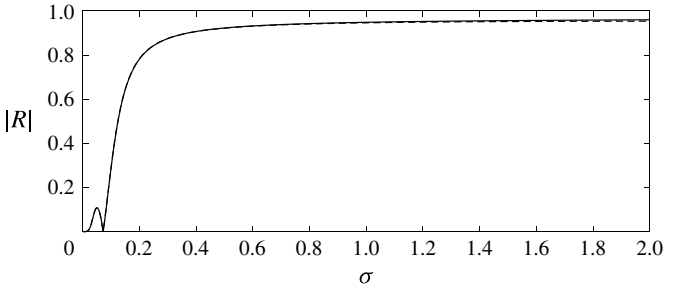


FIGURE 2. Comparison of reflection coefficients. Solid line: R_c for a crack; dashed line: R_p for a polynya with $b = 0.05$. ($H = 100$, $h = 1$, $m = 0.9$, $L = 45582$.)

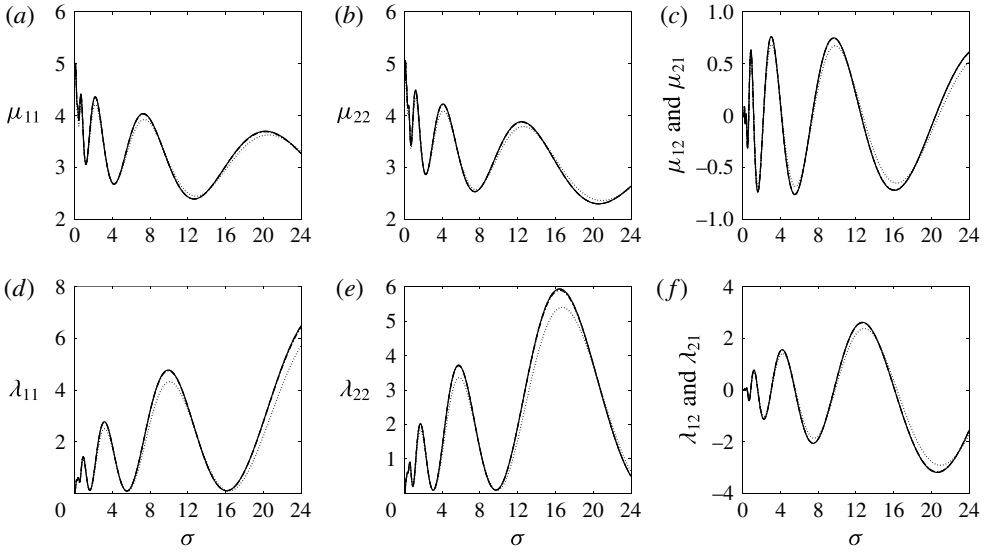


FIGURE 3. Hydrodynamic coefficients of a submerged circular cylinder against σ with different N. Solid lines: $N = 7$; dashed lines: $N = 5$; dash-dotted lines: $N = 3$; dotted lines: $N = 1$. ($a = 1$, $x_0 = 20$, $z_0 = -1.2$, $H = 20$, $h = 0.2$, $m = 0.18$, $L = 72.932$.)

4.2. *The radiation problem*

We consider the radiation problem of a submerged circular cylinder, with its radius a taken as the characteristic length. The convergence study with N is first carried out through the hydrodynamic coefficients against $\sigma = \omega^2 a/g$, as presented in figure 3. It can be seen that the numerical results converge very rapidly, and $N = 5$ and $N = 7$ give graphically indistinguishable results in the figure. The far field formula in the appendix has been used for calculating the damping coefficient and excellent agreement with the near field result has been found. For the results obtained subsequently we have taken $N = 5$.

In figure 4 we show the hydrodynamic coefficients at different x_0. As can be observed in this figure, when $\sigma \to 0$, the results with the crack will tend to those without the crack. This is due to the fact that at very small σ, the condition in (2.3) tends to $\partial\phi_j/\partial z = 0$ on $z = 0$, which means $\partial^3\phi_j/\partial z\partial x^2 \to 0$ and $\partial^4\phi_j/\partial z\partial x^3 \to 0$ on the whole ice sheet. Therefore, the conditions at the crack will be automatically satisfied.

https://doi.org/10.1017/jfm.2018.265 Published online by Cambridge University Press

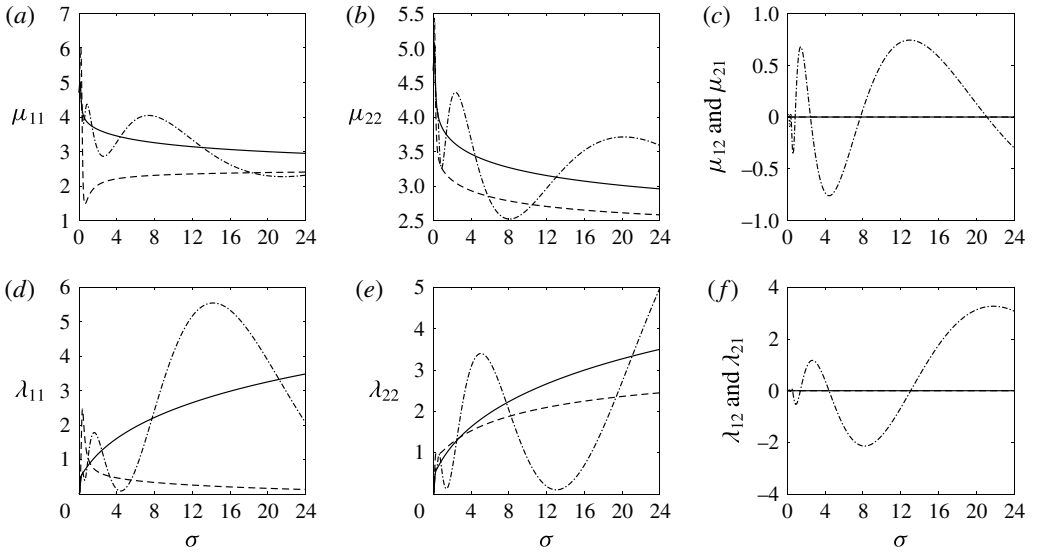


FIGURE 4. Hydrodynamic coefficients of a submerged circular cylinder against σ at different x_0. Solid lines: ice sheet without crack; dashed lines: $x_0 = 0$; dash-dotted lines: $x_0 = 10$. ($a = 1,\ z_0 = -1.2,\ H = 20,\ h = 0.2,\ m = 0.18,\ L = 72.932$.)

Also as $\sigma \to 0$, the effect of the position of x_0 diminishes. When $x_0 = 0$, we have $\mathcal{G}_1(n) = \mathcal{G}_2(n)$ in (3.45*a*) and (3.45*b*), which means in (3.50*a*)–(3.50*c*) $C(n, l) = C(l, n)$ and $D(n, l) = E(n, l)$. Then (3.52) and (3.53) give

$$A_l^1 + B_l^1 = 0, \quad A_l^2 - B_l^2 = 0. \tag{4.7a,b}$$

This suggests that ϕ_1 and ϕ_2 in (3.46) are antisymmetric and symmetric about the body centre respectively, as fully expected. Therefore, we have τ_{js} equal to zero when $j \neq s$.

We may notice in figure 4 that when $x_0 \neq 0$, the results are oscillatory with the frequency. Obviously, this is due to the fact that the wave generated by the body motion will arrive at the crack and then be reflected back to the body. This process is very much frequency dependent. Also we may infer that if we move the body position from x_0 to $x_0 + \ell/2$, where $\ell = 2\pi/\lambda$ is the wavelength of the travelling wave generated by the body, the effect of the crack may be almost the same. To verify that, in figure 5 we plot μ_{22} and λ_{22} against $\Lambda = \lambda x_0$ at various σ, or a fixed λ when x_0 varies. It can be seen that the results become virtually periodic with x_0 when $\Lambda > 4$ and they also become graphically indistinguishable to those from wide approximation method. To provide further insight into what has been observed in figure 5, we may follow the procedure in Li *et al.* (2017*a*) and use the equations in § 3.5.1.

Similar to (B 4), $f_{E,j}^o$ for the ice sheet without the crack can be expressed through the far field formula as

$$f_{E,j}^o = 2I\rho\omega Q_0 C_g A_j^-, \tag{4.8}$$

where Q_0 and C_g are given in (A 7) and (A 8) respectively. Then invoking (3.81), we have

$$\tau_{js} = \tau_{js}^o + 2\mathrm{i}\rho Q_0 C_g A_{js}, \tag{4.9}$$

https://doi.org/10.1017/jfm.2018.265 Published online by Cambridge University Press

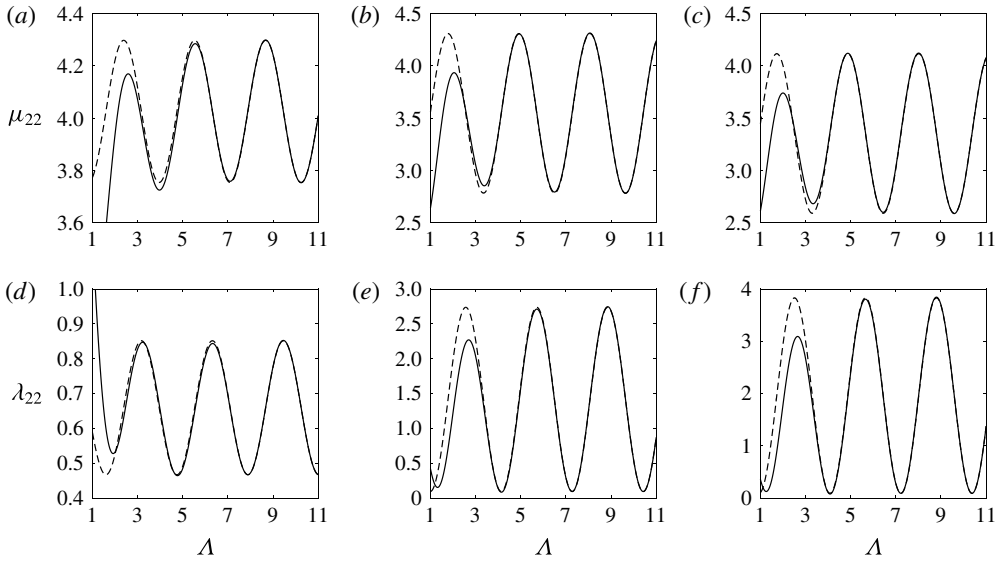


FIGURE 5. Hydrodynamic coefficients of a submerged circular cylinder against Λ in heave mode. In (*a*) and (*d*), $\sigma = 0.50$; in (*b*) and (*e*), $\sigma = 3.00$; in (*c*) and (*f*), $\sigma = 6.00$. Solid line is for the exact results, while dashed line denotes the results from wide spacing approximation. ($a = 1,\ z_0 = -1.2,\ H = 20,\ h = 0.2,\ m = 0.18,\ L = 72.932$.)

where

$$A_{js} = \frac{A_j^- A_s^- R_c}{\mathrm{e}^{2\mathrm{i}\Lambda} - R_c r_0}. \tag{4.10}$$

For a given σ, (4.10) shows that A_{js} is periodic against x_0 with period of $\ell/2$. This means that μ_{js} and λ_{js} both will respectively have the same values at $x_0 + n\ell/2$, where n includes all integers to ensure that x_0 is positive. From (4.10) it can be also seen that A_{js} maps the unit circle $\mathrm{e}^{2\mathrm{i}\Lambda}$ to a circle with centre at

$$y_{c,r} = x_{c,r} + \mathrm{i}z_{c,r} = -|R_c r_0| r_r \mathrm{e}^{\mathrm{i}\vartheta_r}, \tag{4.11}$$

and radius as

$$r_r = \frac{|A_j^- A_s^- R_c|}{1 - |R_c r_0|^2}, \tag{4.12}$$

where

$$\mathrm{e}^{\mathrm{i}\vartheta_r} = \frac{A_j^- A_s^- \bar{r}_0}{|A_j^- A_s^- \bar{r}_0|}. \tag{4.13}$$

From (4.11) and (4.12), (4.10) can be rewritten as

$$A_{js} = y_{c,r} + r_r \mathrm{e}^{\mathrm{i}\tau_r}. \tag{4.14}$$

This indicates that the peak (+) and trough (−) of μ_{js} respectively equal

$$\mu_{js}^{\pm} = \mu_{js}^{o} - 2\rho Q_0 C_g (z_{c,r} \mp r_r), \tag{4.15}$$

https://doi.org/10.1017/jfm.2018.265 Published online by Cambridge University Press

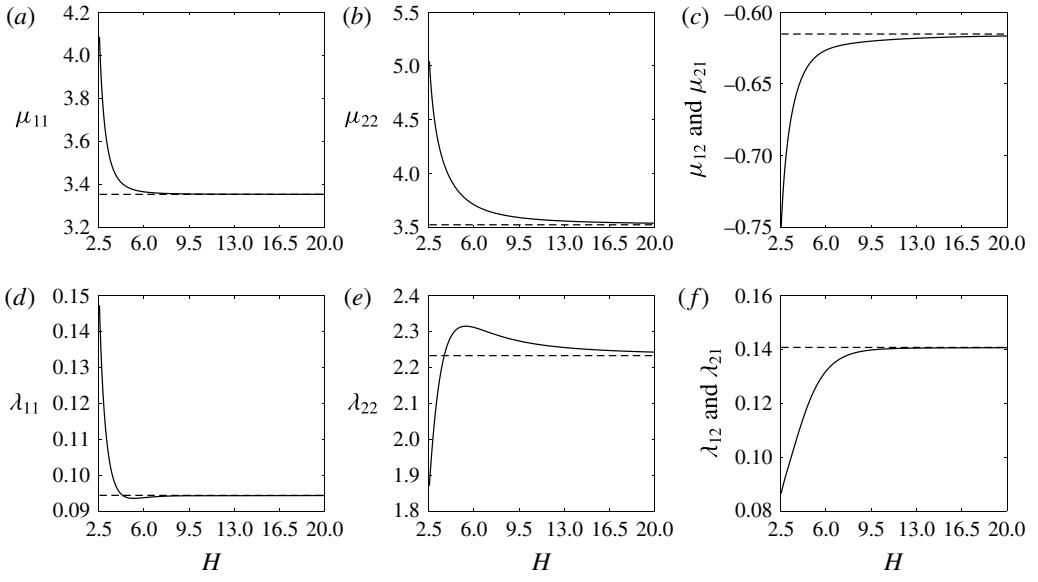


FIGURE 6. Hydrodynamic coefficients of a submerged circular cylinder against H. Solid line represents the results by the method for finite water depth, while dashed line represents those by the method for infinite water depth. ($a = 1$, $(x_0, z_0) = (5.0, -1.2)$, $\sigma = 3.00$, $h = 0.2$, $m = 0.18$, $L = 72.932$.)

and they occur respectively when τ_r equals $-\pi/2$ or $\pi/2$. Similarly, the peak $(+)$ and trough $(-)$ of λ_{js} respectively equal

$$\lambda_{js}^{\pm} = \lambda_{js}^{o} - 2\omega\rho Q_0 C_g(x_{c,r} \mp r_r), \tag{4.16}$$

and they occur respectively when τ_r equals π or 0. We may notice that the corresponding Λ for $\mu_{js}^{\pm}$ and $\lambda_{js}^{\pm}$ can be further obtained from (4.10) and (4.14).

The above discussions are valid for a body of general shape. For the circular cylinder, (4.10) may be further simplified. As shown in § 3.5.2, $|r_0|$ is zero for infinite water depth. For the finite water depth neither $\mu_l(0)$ nor $E(n, l)$ is zero, and $|r_0|$ will not exactly be zero. However, $|r_0|$ is still much smaller than $|t_0|$. In fact it has been found that $|r_0| < 0.01$ over the range of σ in figures 4 and 5. Thus (4.10) can be approximated as

$$A_{js} \approx A_j^- A_s^- R_c \mathrm{e}^{-2\mathrm{i}\Lambda}, \tag{4.17}$$

which gives $y_{c,r} \approx 0$ and $r_r \approx |A_j^- A_s^- R_c|$. These indicate that the local extrema of μ_{js} and λ_{js} will appear when A_{js} respectively becomes a purely imaginary or real number, and if one of them reaches a local extremum, the other will reach the value for ice sheet without the crack.

In figure 6, we show the hydrodynamic coefficients against H for a given σ. As can be expected, the results tend to those for infinite water depth as H becomes larger. However for the heave mode, or $j = 2$, it can be seen that this trend is very slow.

For the problem of a free surface with infinite water depth, Ogilvie (1963) found that the wave generated by the forced body oscillation would propagate only in one direction if the path of the circular cylinder centre follows a circular orbit. When the water surface is covered by an ice sheet, a similar conclusion may be drawn.

https://doi.org/10.1017/jfm.2018.265 Published online by Cambridge University Press

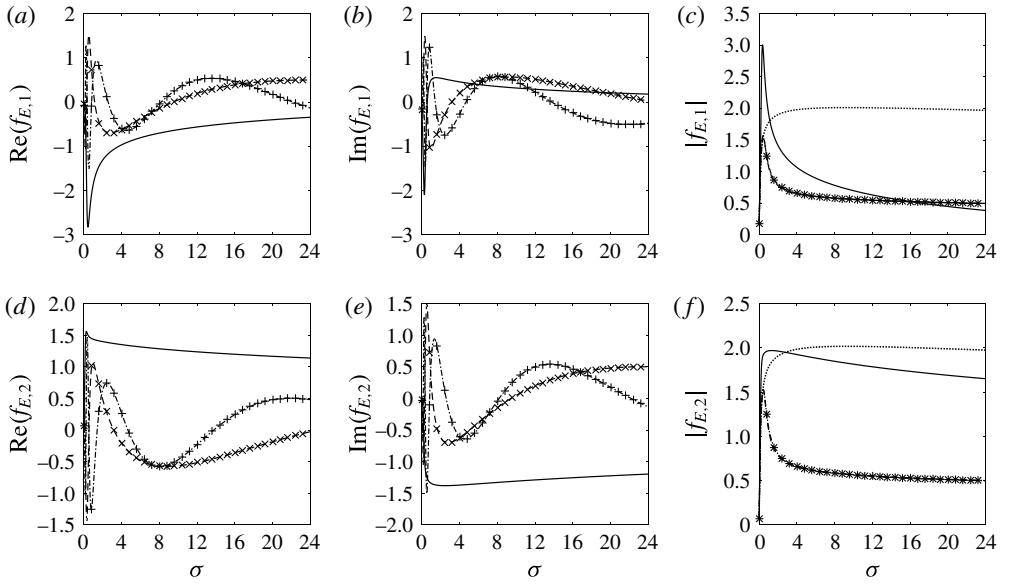


FIGURE 7. Wave exciting force on a submerged circular cylinder against σ at different x_0. Solid lines: $x_0 = 0$; dashed lines: $x_0 = 10$; dash-dotted lines: $x_0 = 20$; dotted lines: ice sheet without crack. $\times$ and $+$ are the wide spacing solutions for $x_0 = 10$ and $x_0 = 20$, respectively. ($a = 1$, $z_0 = -1.2$, $H = 20$, $h = 0.2$, $m = 0.18$, $L = 72.932$.)

Removing the terms related to $\mathcal{I}_1$ and $\mathcal{I}_2$ in (3.50*a*)–(3.50*c*) and noticing (3.92*a*)–(3.92*c*), invoking (3.52) we have

$$A_l^2 = \mathrm{i}A_l^1. \tag{4.18}$$

We may take the clockwise rotation as an example. This is achieved by taking the motion amplitudes $|\alpha_1| = |\alpha_2|$ in (2.1), and their phases $\vartheta_2 = \vartheta_1 + \pi/2$. Invoking (3.46) and (4.18) we obtain

$$\Phi(x, z, t) = \mathrm{Re}\left[\mathrm{i}\omega \mathrm{e}^{\mathrm{i}\omega t}\alpha_1 \sum_{n=1}^{\infty} a^n (B_n^1 \mathrm{e}^{\mathrm{i}\vartheta_1} + \mathrm{i}B_n^2 \mathrm{e}^{\mathrm{i}\vartheta_1}) g_n\right]. \tag{4.19}$$

Since $\lim_{x\to-\infty} g_n = 0$, we can conclude that clockwise oscillation will generate the wave propagating to $x = +\infty$ only. Similarly, the counterclockwise oscillation will generate the wave propagating to $x = -\infty$ only due to $\lim_{x\to+\infty} f_n = 0$. When there is a crack in the ice sheet, since the equations for A_l^j and B_l^j are coupled, (4.18) is not valid in general. However, when $x_0 \to +\infty$, we have $\mathcal{G}_2(n) \to 0$ in (3.91*b*), which gives $E(n, l) \to 0$ in (3.50*c*). Substituting this into (3.52), we can obtain (4.18) again, i.e. no wave will propagate to $x = -\infty$ for clockwise oscillation.

4.3. *The diffraction problem*

We then consider the problem of wave diffraction by the submerged circular cylinder. Figure 7 presents the results for the excitation force at different x_0 against σ, together with those for the ice sheet without crack. From each figure, it can be seen that

https://doi.org/10.1017/jfm.2018.265 Published online by Cambridge University Press

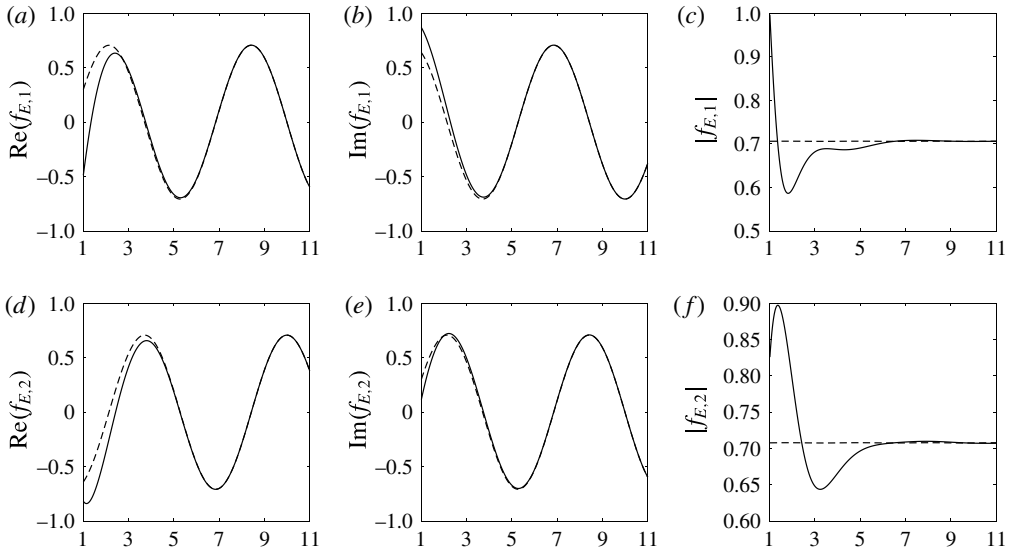


FIGURE 8. Wave exciting force on a submerged circular cylinder against Λ. Solid line is for the exact results, while dashed line denotes the results from wide spacing approximation. ($a = 1,\ z_0 = -1.2,\ \sigma = 3.00,\ H = 20,\ h = 0.2,\ m = 0.18,\ L = 72.932$.)

the results tend to the same value when $\sigma \to 0$, for the reason discussed in § 4.2. It can also be seen that when x_0 is sufficiently large, the exact results are hardly different from those from the wide spacing method in § 3.5.1, even for very long waves, although the approximation is based on the assumption that x_0 is much larger than the wavelength. The reason for that is when $\sigma \to 0$, $\epsilon_0 \to 1$. Then invoking (3.86) we have that $f_{E,j}$ tends to $f^o_{E,j}$, or it tends to the exact result. This reveals that the wide spacing approximation can work well for both small and large σ.

We may use the wide spacing approximation in (3.86) to give some insights into the features of the wave exciting force. Substituting (3.84) into (3.86) and invoking (4.8), we obtain

$$f_{E,j} = -2\mathrm{i}\rho g Q_0 C_g (A_j^- \epsilon_0 \mathrm{e}^{\mathrm{i}\Lambda})\mathrm{e}^{-\mathrm{i}\Lambda}. \tag{4.20}$$

Here

$$A_j^- \epsilon_0 \mathrm{e}^{\mathrm{i}\Lambda} = \frac{A_j^- T_c \mathrm{e}^{2\mathrm{i}\Lambda}}{\mathrm{e}^{2\mathrm{i}\Lambda} - R_c r_0}. \tag{4.21}$$

It should be noticed that the oscillatory term $A_j^- \epsilon_0 \mathrm{e}^{\mathrm{i}\Lambda}$ is due to the interaction between the cylinder and the crack, while the oscillatory term $\mathrm{e}^{-\mathrm{i}\Lambda}$ is due to the initial phase of the incident potential ϕ_I relative to the body at x_0. From (4.20), we can see that at a fixed σ, $f_{E,j}$ is periodic against Λ or it varies periodically with x_0. The period for $\mathrm{Re}(f_{E,j})$ and $\mathrm{Im}(f_{E,j})$ equals 2π, as can be observed in figure 8.

From (4.21) it can be seen that $A_j^- \epsilon_0 \mathrm{e}^{\mathrm{i}\Lambda}$ maps the unit circle $\mathrm{e}^{2\mathrm{i}\Lambda}$ to a circle with centre at

$$y_{c,d} = x_{c,d} + \mathrm{i}z_{c,d} = \frac{|1 - 2|R_c r_0|^2|}{|R_c r_0|} r_d \mathrm{e}^{\mathrm{i}\vartheta_d}, \tag{4.22}$$

and radius as

$$r_d = \frac{|A_j^- T_L R_c r_0|}{1 - |R_c r_0|^2}, \tag{4.23}$$

https://doi.org/10.1017/jfm.2018.265 Published online by Cambridge University Press

where

$$e^{i\vartheta_d} = \frac{(1-2|R_c r_0|^2)A_j^- T_c}{|(1-2|R_c r_0|^2)A_j^- T_c|}. \tag{4.24}$$

From (4.22) and (4.23), (4.21) can be rewritten as

$$A_j^- \epsilon_0 e^{i\Lambda} = y_{c,d} + r_d e^{i\tau_d}. \tag{4.25}$$

This indicates that the peak (+) and trough (−) of $|f_{E,j}|$ respectively equal

$$|f_{E,j}^{\pm}| = 2\rho g Q_0 C_g ||y_{c,d}| \pm r_d|, \tag{4.26}$$

and they occur respectively when τ_d equals ϑ_d or $\vartheta_d + \pi$, and the corresponding Λ can be further obtained according to (4.21) and (4.25). For the special case $1-2|R_c r_0|^2 = 0$, we have $y_{c,d} = 0$ and $|f_{E,j}^+| = |f_{E,j}^-|$, which means that the location of the cylinder no longer has an effect on the magnitude of the force and the magnitude of the force is no longer oscillatory with respect to x_0.

We may notice that the above discussions are valid for a body of generalized shape. For the present case of a circular cylinder, we may use the fact that $r_0 \approx 0$. Equation (4.21) becomes

$$A_j^- \epsilon_0 e^{i\Lambda} \approx A_j^- T_c. \tag{4.27}$$

Substituting (4.27) into (4.20), it can be found that the oscillations of $\mathrm{Re}(f_{E,j})$ and $\mathrm{Im}(f_{E,j})$ in figure 8 are purely due to the fact that the cylinder is placed at a different horizontal position which causes the relative phase change of the incident wave. The magnitude of the exciting force becomes $|f_{E,j}| = 2\rho g Q_0 C_g |A_j^- T_c|$, which is not affected by x_0, as can be seen in figure 8. We may notice that although $|f_{E,j}|$ tends to a constant as x_0 increases, the value of the constant is different from the force on the body without a crack. This is because ϕ_D^1 in (3.61) at the body does not tend to zero even when $x_0 \to +\infty$. In fact, we have $|f_{E,j}| < |f_{E,j}^o|$ because $|T_c| < 1$ is always valid based on the energy conservation equation (Barrett & Squire 1996).

5. Conclusions

The solution for the wave radiation and diffraction by a circular cylinder submerged below an ice sheet with a crack has been presented. The Green function satisfying both the ice sheet and the crack conditions is obtained in an integral form. By using this Green function, the solution for the problem of wave diffraction by the crack in the absence of the body is solved directly. The solution for each multipole is derived directly from the differentiation of the Green function with respect to the source position, from which the velocity potential for a submerged circular cylinder is constructed.

For the solution of wave diffraction by a polynya, results show that the reflection coefficient tends to that of a crack when the polynya width tends to zero. The hydrodynamic coefficients and exciting force of a submerged cylinder are found to be quite oscillatory with the frequency when the body is not right below the crack. However, the oscillation of the exciting force is observed only in its real and imaginary parts separately and there is no strong oscillation in the magnitude of the force. When the cylinder is away from the crack, accurate solution can be obtained through the wide spacing approximation method. From this method, it is shown explicitly that at a given frequency, the hydrodynamic coefficients, and the real and imaginary parts of the exciting force vary periodically with the distance

https://doi.org/10.1017/jfm.2018.265 Published online by Cambridge University Press

between the cylinder and crack. This means that the effect of the crack always exists even when the distance tends to infinity. It can therefore be expected that the motion amplitude of the body will be quite oscillatory with the wave frequency and with the location of the crack, as in the case of polynya (Li *et al.* 2018), which has important implications for the performance of a marine vehicle in ice covered waters.

The Green function derived in this work also has much wider applications apart from being used as the starting point for the multipole expansion in the paper. Its simple form allows the function to be evaluated efficiently, instead of through solving a large matrix equation obtained from truncations of infinite series repeatedly for the source at each different position, as done in the previous work. The derived Green function allows the traditional method of source distribution over the body surface in the free surface flow problem to be used directly for a body submerged below an ice sheet with a crack. This makes the simulation for a cross-section of a realistic ship possible.

The solution procedure can be further extended to other forms of crack conditions, e.g. hinged or connected by springs, which may have practical implications in wave power absorptions or hydroelasticities. The solution procedure can be also used as a base for the derivation of a solution for an ice sheet with multiple cracks. However, the method is limited to the case in which the physical properties of the ice sheet are constant. It should be also mentioned that the analysis is within the scope of the linear velocity potential theory, which is not valid when the incoming wave amplitude or the body motion amplitude is large compared with the wavelength or the body dimension.

Acknowledgements

This work is supported by Lloyd's Register Foundation through the joint centre involving University College London, Shanghai Jiaotong University and Harbin Engineering University, to which the authors are most grateful. Lloyd's Register Foundation helps to protect life and property by supporting engineering-related education, public engagement, and the application of research. This work is also supported by the National Natural Science Foundation of China (grant nos 11472088 and 51709131).

Appendix A. The far field formula for the damping coefficient

From (3.56), we have

$$\tau_{js} - \tau_{sj} = \rho \int_{S_0} \left(\phi_s \frac{\partial \phi_j}{\partial n} - \phi_j \frac{\partial \phi_s}{\partial n} \right) \mathrm{d}S. \tag{A 1}$$

The integral over the body surface S_0 can be converted into the rest of the fluid boundary through Green's identity. By using the corresponding boundary conditions, we can obtain $\tau_{js} - \tau_{sj} = 0$, or

$$\mu_{js} = \mu_{sj}, \quad \lambda_{js} = \lambda_{sj}. \tag{A 2a,b}$$

For the damping coefficient λ_{js}, (3.56) gives

$$-\frac{2\mathrm{i}}{\omega}\lambda_{js} = \rho \int_{S_0} \left(\phi_s \frac{\partial \bar{\phi}_j}{\partial n} - \bar{\phi}_j \frac{\partial \phi_s}{\partial n} \right) \mathrm{d}S, \tag{A 3}$$

https://doi.org/10.1017/jfm.2018.265 Published online by Cambridge University Press

where the overbar means conjugation. This integral can be converted to the rest of the fluid boundary and it will become

$$-\frac{2\mathrm{i}}{\omega}\lambda_{js} = -\rho\int_{S_{+\infty}+S_{-\infty}}\left(\phi_s\frac{\partial\bar{\phi}_j}{\partial n}-\bar{\phi}_j\frac{\partial\phi_s}{\partial n}\right)\mathrm{d}S$$
$$-\frac{L}{\omega^2}\left[\left(\frac{\partial^4\phi_s}{\partial x^3\partial z}\frac{\partial\bar{\phi}_j}{\partial z}-\frac{\partial^3\phi_s}{\partial x^2\partial z}\frac{\partial^2\bar{\phi}_j}{\partial x\partial z}+\frac{\partial^3\bar{\phi}_j}{\partial x^2\partial z}\frac{\partial^2\phi_s}{\partial x\partial z}-\frac{\partial^4\bar{\phi}_j}{\partial x^3\partial z}\frac{\partial\phi_s}{\partial z}\right)_{z=0}\right]_{x=-\infty}^{x=+\infty}, \quad (A\,4)$$

once the boundary conditions on the bottom and ice sheet, and at the crack have been used. Here, $S_{\pm\infty}$ are two vertical lines located at $x=\pm\infty$ respectively. We may write the asymptotic expression of ϕ_j as

$$\phi_j = \begin{cases} R_j^+\mathrm{e}^{-\mathrm{i}\lambda x}\psi(z) & \text{at } x\to+\infty \\ R_j^-\mathrm{e}^{+\mathrm{i}\lambda x}\psi(z) & \text{at } x\to-\infty. \end{cases} \quad (A\,5)$$

Substituting this into (A 4), we have

$$\lambda_{js} = (R_s^-\bar{R_j^-}+R_s^+\bar{R_j^+})\rho\omega Q_0 C_g, \quad (A\,6)$$

where

$$Q_0 = \frac{\rho\omega(L\lambda^4+\rho g)}{(L\lambda^4+\rho g-m\omega^2)^2}, \quad (A\,7)$$

and

$$C_g = \frac{2L\lambda^3\omega}{L\lambda^4+\rho g}+\frac{\omega}{2\lambda}\left[1+\frac{2\lambda H}{\sinh(2\lambda H)}\right]\frac{L\lambda^4+\rho g-m\omega^2}{L\lambda^4+\rho g} \quad (A\,8)$$

is the group velocity for the flexural gravity wave. The radiation coefficients R_j^+ and R_j^- in (A 6) can be obtained by letting $x\to\pm\infty$ in (3.46). We have

$$R_j^+ = \frac{\mathrm{i}\pi}{K'(\omega,\lambda)}\sum_{n=1}^{\infty}\frac{a^n}{(n-1)!}\left\{A_n^j\left\{2(-\lambda)^{n-1}\mathrm{e}^{-\lambda(z_0+2H)+\mathrm{i}\lambda x_0}\right.\right.$$
$$\times[(L\lambda^4+\rho g-m\omega^2)\lambda+\rho\omega^2]+L\rho\omega^2\lambda^2\left[\frac{\lambda\mathcal{G}_1(n)}{\mathcal{I}_1}-\frac{\mathcal{G}_1(n-1)}{\mathcal{I}_2}\right]\Big\}$$
$$-B_n^j\left\{2\lambda^{n-1}\mathrm{e}^{\lambda z_0+\mathrm{i}\lambda x_0}\right.$$
$$\left.\left.\times[(L\lambda^4+\rho g-m\omega^2)\lambda+\rho\omega^2]+L\rho\omega^2\lambda^2\left[\frac{\lambda\mathcal{G}_2(n)}{\mathcal{I}_1}+\frac{\mathcal{G}_2(n-1)}{\mathcal{I}_2}\right]\right\}\right\}, \quad (A\,9)$$

and

$$R_j^- = \frac{\mathrm{i}\pi}{K'(\omega,\lambda)}\sum_{n=1}^{\infty}\frac{a^n}{(n-1)!}\left\{A_n^j\left\{-2\lambda^{n-1}\mathrm{e}^{\lambda z_0-\mathrm{i}\lambda x_0}\right.\right.$$
$$\times[(L\lambda^4+\rho g-m\omega^2)\lambda+\rho\omega^2]-L\rho\omega^2\lambda^2\left[\frac{\lambda\mathcal{G}_1(n)}{\mathcal{I}_1}+\frac{\mathcal{G}_1(n-1)}{\mathcal{I}_2}\right]\Big\}$$
$$+B_n^j\left\{2(-\lambda)^{n-1}\mathrm{e}^{-\lambda(z_0+2H)-\mathrm{i}\lambda x_0}\right.$$
$$\left.\left.\times[(L\lambda^4+\rho g-m\omega^2)\lambda+\rho\omega^2]+L\rho\omega^2\lambda^2\left[\frac{\lambda\mathcal{G}_2(n)}{\mathcal{I}_1}-\frac{\mathcal{G}_2(n-1)}{\mathcal{I}_2}\right]\right\}\right\}, \quad (A\,10)$$

where the prime in $K'(\omega,\lambda)$ denotes partial derivative with respect to λ.

https://doi.org/10.1017/jfm.2018.265 Published online by Cambridge University Press

Appendix B. The far field formula for the wave exciting force

By noticing the condition in (2.5), the wave exciting force in (3.72) can be given as

$$f_{E,j} = -\mathrm{i}\omega\rho \int_{S_0} \left(\phi_0 \frac{\partial \phi_j}{\partial n} - \phi_j \frac{\partial \phi_0}{\partial n} \right) \mathrm{d}S. \tag{B 1}$$

As for the damping coefficient, this can be converted as

$$\begin{aligned} f_{E,j} = {} & \mathrm{i}\omega\rho \int_{S_{+\infty}+S_{-\infty}} \left(\phi_0 \frac{\partial \phi_j}{\partial n} - \phi_j \frac{\partial \phi_0}{\partial n} \right) \mathrm{d}S \\ & + \mathrm{i}\frac{L}{\omega} \left[\left(\frac{\partial^4 \phi_0}{\partial x^3 \partial z} \frac{\partial \phi_j}{\partial z} - \frac{\partial^3 \phi_0}{\partial x^2 \partial z} \frac{\partial^2 \phi_j}{\partial x \partial z} + \frac{\partial^3 \phi_j}{\partial x^2 \partial z} \frac{\partial^2 \phi_0}{\partial x \partial z} - \frac{\partial^4 \phi_j}{\partial x^3 \partial z} \frac{\partial \phi_0}{\partial z} \right)_{z=0} \right]_{x=-\infty}^{x=+\infty}. \end{aligned} \tag{B 2}$$

At $x \to \pm\infty$, ϕ_0 can be written in the following asymptotic form

$$\phi_0 = \begin{cases} T\mathrm{e}^{-\mathrm{i}\lambda x}\psi(z) & \text{at } x \to +\infty \\ (I\mathrm{e}^{-\mathrm{i}\lambda x} + R\mathrm{e}^{+\mathrm{i}\lambda x})\psi(z) & \text{at } x \to -\infty. \end{cases} \tag{B 3}$$

Thus (B 2) becomes

$$f_{E,j} = 2I\rho\omega Q_0 C_g R_j^-. \tag{B 4}$$

The transmission and reflection coefficients in (B 3) can be obtained by letting $x \to \pm\infty$ in (3.46) and (3.66). We obtain

$$T = T_0 + I \times T_c, \tag{B 5}$$

$$R = R_0 + I \times R_c, \tag{B 6}$$

where T_0 and R_0 are due to ϕ_D^2 and can be obtained through equations similar to (A 9) and (A 10); T_c and R_c are due to ϕ_D^1 and can be obtained from (3.66)

$$T_c = 1 + \frac{\mathrm{i}\pi}{K'(\omega, \lambda)} L\lambda^5 \tanh(\lambda H) \left(\frac{\lambda^2}{\mathcal{I}_1} + \frac{1}{\mathcal{I}_2} \right), \tag{B 7}$$

$$R_c = -\frac{\mathrm{i}\pi}{K'(\omega, \lambda)} L\lambda^5 \tanh(\lambda H) \left(\frac{\lambda^2}{\mathcal{I}_1} - \frac{1}{\mathcal{I}_2} \right). \tag{B 8}$$

Appendix C. Haskind relation for wave exciting force

Substituting $\varphi = \phi_I + \phi_D^1$ and ϕ_D^2 into (3.72), and noticing the condition in (2.5), we can write the wave exciting force as

$$f_{E,j} = -\mathrm{i}\omega\rho \int_{S_0} \left(\varphi \frac{\partial \phi_j}{\partial n} + \phi_D^2 \frac{\partial \phi_j}{\partial n} \right) \mathrm{d}S. \tag{C 1}$$

Applying Green's second identity to ϕ_D^2 and ϕ_j over the fluid boundary S, we have

$$0 = \int_S \left(\phi_D^2 \frac{\partial \phi_j}{\partial n} - \phi_j \frac{\partial \phi_D^2}{\partial n} \right) \mathrm{d}S. \tag{C 2}$$

https://doi.org/10.1017/jfm.2018.265 Published online by Cambridge University Press

Noticing that both ϕ_D^2 and ϕ_j represent the outgoing wave at infinity and satisfy the ice sheet and seabed conditions, we can rewrite (C 2) as

$$0 = \int_{S_0} \left(\phi_D^2 \frac{\partial \phi_j}{\partial n} - \phi_j \frac{\partial \phi_D^2}{\partial n} \right) \mathrm{d}S + \frac{L}{\rho \omega^2} \left[\left(\frac{\partial^4 \phi_D^2}{\partial x^3 \partial z} \frac{\partial \phi_j}{\partial z} - \frac{\partial^3 \phi_D^2}{\partial x^2 \partial z} \frac{\partial^2 \phi_j}{\partial x \partial z} + \frac{\partial^3 \phi_j}{\partial x^2 \partial z} \frac{\partial^2 \phi_D^2}{\partial x \partial z} - \frac{\partial^4 \phi_j}{\partial x^3 \partial z} \frac{\partial \phi_D^2}{\partial z} \right)_{z=0} \right]_{x=0^+}^{x=0^-}. \tag{C 3}$$

Through the condition in (2.4) for ϕ_D^2 and ϕ_j at the crack, (C 3) gives

$$\int_{S_0} \left(\phi_D^2 \frac{\partial \phi_j}{\partial n} \right) \mathrm{d}S = \int_{S_0} \left(\phi_j \frac{\partial \phi_D^2}{\partial n} \right) \mathrm{d}S. \tag{C 4}$$

Substituting this into (C 1) and noticing the condition in (3.69), we can obtain the Haskind relation for $f_{E,j}$ as

$$f_{E,j} = -\mathrm{i}\omega\rho \int_{S_0} \left(\varphi \frac{\partial \phi_j}{\partial n} - \phi_j \frac{\partial \varphi}{\partial n} \right) \mathrm{d}S, \tag{C 5}$$

which is similar to that for an infinitely extended free surface (Mei, Stiassnie & Yue 2005). It should be noticed that in the free surface problem φ includes the incident potential ϕ_I from infinity only, while in (C 5) φ contains not only ϕ_I but also its diffraction potential ϕ_D^1 by the crack.

REFERENCES

Abramowitz, M. & Stegun, I. A. 1965 *Handbook of Mathematical Functions*. Dover.

Balmforth, N. J. & Craster, R. V. 1999 Ocean waves and ice sheets. *J. Fluid Mech.* **395**, 89–124.

Barrett, M. D. & Squire, V. A. 1996 Ice-coupled wave propagation across an abrupt change in ice rigidity, density, or thickness. *J. Geophys. Res. Oceans* **101** (C9), 20825–20832.

Chung, H. & Fox, C. 2002 Calculation of wave-ice interaction using the wiener-hopf technique. *New Zealand J. Math.* **31** (1), 1–18.

Chung, H. & Linton, C. M. 2005 Reflection and transmission of waves across a gap between two semi-infinite elastic plates on water. *Q. J. Mech. Appl. Maths* **58** (1), 1–15.

Das, D. & Mandal, B. N. 2006 Oblique wave scattering by a circular cylinder submerged beneath an ice-cover. *Intl J. Engng Sci.* **44** (3–4), 166–179.

Dean, W. R. 1948 On the reflexion of surface waves by a submerged circular cylinder. *Math. Proc. Camb. Phil. Soc.* **44** (4), 483–491.

Evans, D. V. & Davies, T. V. 1968 Wave-ice Interaction. *Report*. Davidson Laboratory, Stevens Institute of Technology.

Evans, D. V. & Porter, R. 2003 Wave scattering by narrow cracks in ice sheets floating on water of finite depth. *J. Fluid Mech.* **484**, 143–165.

Faltinsen, O. M. 2005 *Hydrodynamics of High-speed Marine Vehicles*. Cambridge University Press.

Fox, C. & Squire, V. A. 1990 Reflection and transmission characteristics at the edge of shore fast sea ice. *J. Geophys. Res. Oceans* **95** (C7), 11629–11639.

Fox, C. & Squire, V. A. 1994 On the oblique reflexion and transmission of ocean waves at shore fast sea ice. *Phil. Trans. R. Soc.* A **347** (1682), 185–218.

Greenhill, A. G. 1887 Wave motion in hydrodynamics. *Am. J. Maths* **9** (1), 62–96.

https://doi.org/10.1017/jfm.2018.265 Published online by Cambridge University Press

LI, Z. F., SHI, Y. Y. & WU, G. X. 2017*a* Interaction of wave with a body floating on a wide polynya. *Phys. Fluids* **29** (9), 097104.

LI, Z. F., SHI, Y. Y. & WU, G. X. 2017*b* Large amplitude motions of a submerged circular cylinder in water with an ice cover. *Eur. J. Mech. (*B*/Fluids)* **65**, 141–159.

LI, Z. F., SHI, Y. Y. & WU, G. X. 2018 Interaction of waves with a body floating on polynya between two semi-infinite ice sheets. *J. Fluids Struct.* **78**, 86–108.

LIGHTHILL, J. 1978 *Waves in Fluids*. Cambridge University Press.

MEI, C. C., STIASSNIE, M. & YUE, K. P. 2005 *Theory and Applications of Ocean Surface Waves Part 1: Linear Aspects*. World Scientific Publishing Co. Pte. Ltd.

MEYLAN, M. & SQUIRE, V. A. 1993 Finite-floe wave reflection and transmission coefficients from a semi-infinite model. *J. Geophys. Res. Atmos.* **981** (C7), 12537–12542.

MEYLAN, M. & SQUIRE, V. A. 1994 The response of ice floes to ocean waves. *J. Geophys. Res. Atmos.* **99** (C1), 891–900.

NEWMAN, J. N. 1977 *Marine Hydrodynamics*. MIT Press.

NOBLE, J. V. 2000 Gauss-legendre principal value integration. *Comput. Sci. Engng* **2** (1), 92–95.

OGILVIE, T. F. 1963 First- and second-order forces on a cylinder submerged under a free surface. *J. Fluid Mech.* **16** (03), 451–472.

PORTER, R. & EVANS, D. V. 2006 Scattering of flexural waves by multiple narrow cracks in ice sheets floating on water. *Wave Motion* **43** (5), 425–443.

PORTER, R. & EVANS, D. V. 2007 Diffraction of flexural waves by finite straight cracks in an elastic sheet over water. *J. Fluids Struct.* **23** (2), 309–327.

REN, K., WU, G. X. & THOMAS, G. A. 2016 Wave excited motion of a body floating on water confined between two semi-infinite ice sheets. *Phys. Fluids* **28** (12), 127101.

SAHOO, T., YIP, T. L. & CHWANG, A. T. 2001 Scattering of surface waves by a semi-infinite floating elastic plate. *Phys. Fluids* **13** (11), 3215–3222.

SMITH, L. C. & STEPHENSON, S. R. 2013 New trans-arctic shipping routes navigable by midcentury. *Proc. Natl Acad. Sci. USA* **110** (13), 1191–1195.

SQUIRE, V. A. 2007 Of ocean waves and sea-ice revisited. *Cold Reg. Sci. Technol.* **49** (2), 110–133.

SQUIRE, V. A. 2011 Past, present and impendent hydroelastic challenges in the polar and subpolar seas. *Phil. Trans. R. Soc.* A **369** (1947), 2813–2831.

SQUIRE, V. A. & DIXON, T. W. 2000 An analytic model for wave propagation across a crack in an ice sheet. *Intl J. Offshore Polar Engng* **10** (3), 173–176.

SQUIRE, V. A., DUGAN, J. P., WADHAMS, P., ROTTIER, P. J. & LIU, A. K. 1995 Of ocean waves and sea ice. *Annu. Rev. Fluid Mech.* **27** (1), 115–168.

SROKOSZ, M. A. & EVANS, D. V. 1979 A theory for wave-power absorption by two independently oscillating bodies. *J. Fluid Mech.* **90** (2), 337–362.

STUROVA, I. V. 2014*a* Vibrations of a circular cylinder submerged in a fluid with a non-homogeneous upper boundary. *Trans. ASME J. Appl. Mech. Tech. Phys.* **55** (3), 394–403.

STUROVA, I. V. 2014*b* Wave generation by an oscillating submerged cylinder in the presence of a floating semi-infinite elastic plate. *Fluid Dyn.* **49** (4), 504–514.

STUROVA, I. V. 2015*a* The effect of a crack in an ice sheet on the hydrodynamic characteristics of a submerged oscillating cylinder. *Z. Angew. Math. Mech. J. Appl. Math. Mech.* **79** (2), 170–178.

STUROVA, I. V. 2015*b* Radiation of waves by a cylinder submerged in water with ice floe or polynya. *J. Fluid Mech.* **784**, 373–395.

TKACHEVA, L. A. 2004 The diffraction of surface waves by a floating elastic plate at oblique incidence. *Z. Angew. Math. Mech. J. Appl. Math. Mech.* **68** (3), 425–436.

TKACHEVA, L. A. 2015 Oscillations of a cylindrical body submerged in a fluid with ice cover. *J. Appl. Mech. Tech. Phys.* **56** (6), 1084–1095.

URSELL, F. 1949 On the heaving motion of a circular cylinder on the surface of a fluid. *Q. J. Mech. Appl. Maths.* **2** (2), 215–231.

URSELL, F. 1950 Surface waves on deep water in the presence of a submerged circular cylinder. *Math. Proc. Camb. Phil. Soc.* **46** (1), 141–152.

https://doi.org/10.1017/jfm.2018.265 Published online by Cambridge University Press

WEHAUSEN, J. V. & LAITONE, E. V. 1960 *Surface Waves*, pp. 446–778. Springer.

WILLIAMS, T. D. & SQUIRE, V. A. 2002 Wave propagation across an oblique crack in an ice sheet. *Intl J. Offshore Polar Engng* **12** (3), 157–162.

WILLIAMS, T. D. & SQUIRE, V. A. 2006 Scattering of flexural-gravity waves at the boundaries between three floating sheets with applications. *J. Fluid Mech.* **569**, 113–140.

WU, G. X. 1993 Hydrodynamic forces on a submerged circular cylinder undergoing large-amplitude motion. *J. Fluid Mech.* **254**, 41–58.

WU, G. X. 1998 Wave radiation and diffraction by a submerged sphere in a channel. *Q. J. Mech. Appl. Maths* **51** (4), 647–666.

WU, G. X. & EATOCK TAYLOR, R. 1987 Hydrodynamic forces on submerged oscillating cylinders at forward speed. *Proc. R. Soc. Lond.* A **414** (1846), 149–170.

https://doi.org/10.1017/jfm.2018.265 Published online by Cambridge University Press